

NASA TECHNICAL NOTE



NASA TN D-2463

NASA TN D-2463

LOAN COPY: RETURN  
AFWL (WLIL-2)  
KIRTLAND AFB, N M

0079556



TECH LIBRARY KAFB, NM

THEORETICAL LAMINAR CONVECTIVE  
HEAT TRANSFER AND BOUNDARY-LAYER  
CHARACTERISTICS ON CONES  
AT SPEEDS TO 24 KM/SEC

*by Gary T. Chapman*  
*Ames Research Center*  
*Moffett Field, Calif.*



THEORETICAL LAMINAR CONVECTIVE HEAT TRANSFER  
AND BOUNDARY-LAYER CHARACTERISTICS  
ON CONES AT SPEEDS TO 24 KM/SEC

By Gary T. Chapman

Ames Research Center  
Moffett Field, Calif.

NATIONAL AERONAUTICS AND SPACE ADMINISTRATION

---

For sale by the Office of Technical Services, Department of Commerce,  
Washington, D.C. 20230 -- Price \$1.75

THEORETICAL LAMINAR CONVECTIVE HEAT TRANSFER  
AND BOUNDARY-LAYER CHARACTERISTICS

ON CONES AT SPEEDS TO 24 KM/SEC

By Gary T. Chapman

Ames Research Center  
Moffett Field, Calif.

SUMMARY

Solutions of the equations of boundary layers without pressure gradient for air in chemical and thermodynamic equilibrium have been obtained for free-stream velocities from 3 to 24 kilometers per second, wall temperatures from 1000° K to 4200° K, boundary-layer pressure levels from 0.1 to 10 atmospheres, and values of the ratio of the kinetic energy per unit mass of the stream at the edge of the boundary layer to the total enthalpy (i.e.,  $u_e^2/2H_e$ ) of from 0 to 0.93. From these solutions the heat transfer, skin friction, boundary-layer thickness, displacement thickness, and momentum thickness were calculated. Simple correlations were obtained for the heat-transfer and skin-friction results. The effects of various flow conditions on these correlations as well as on the noncorrelated results were assessed. A complete tabulation of all the necessary parameters is also included so that additional correlations may be sought.

Besides the presentation of the solutions a procedure is outlined which illustrates how the use of the Crocco equation leads to very good first approximations to start the iteration procedure used in obtaining the present solutions. The use of the Crocco equation to start the iteration procedure results in very rapid convergence to the final solution.

INTRODUCTION

The prospect of manned space flight to the planets has stimulated considerable interest in heat transfer to vehicles returning to earth at speeds considerably higher than escape speed. It has been shown (ref. 1) that radiative heat transfer to blunt shapes can be an important or even the dominant mode of heating in this speed range. A recent study by Allen, Seiff, and Winovich (ref. 2) has shown that the radiative heating and also the total heating can be reduced if sharp or slightly blunted cones are used instead of bluff bodies.

Many studies have been made of the convective heat transfer to the stagnation region of blunt bodies at high speeds (refs. 3, 4, 5, and 6) and to blunt-nosed slender bodies (refs. 7 and 8) through the speed range where



dissociation but little or no ionization occurs. However, boundary layers on cones have not been treated for speeds where dissociation and ionization occur. In reference 2, the method of reference 7 was applied to the boundary layer on high-speed cones, but this required extrapolation well beyond the conditions considered in reference 7. The present study was undertaken to provide a more rigorous treatment of the heat-transfer and boundary-layer characteristics for cones at still higher speeds, where the effects of both dissociation and ionization are important.

Calculated heat transfer, skin friction, and three boundary-layer thicknesses are presented for equilibrium flow over sharp cones. These solutions are compared with the Crocco equation for real gas; and a procedure is developed for using the Crocco equation as a starting point in solving the more general boundary-layer equations.

#### SYMBOLS

a,b,m	skin-friction correlation constants
$C_{Df}$	skin-friction drag coefficient
$C_F$	average skin-friction coefficient
$c_f$	local skin-friction coefficient
$c_p$	total specific heat (including the chemical reaction terms)
f,g	normalized variables defined by equation (8)
H	total enthalpy, $h + \frac{u^2}{2}$
h	static enthalpy
$K(p_e, T_w)$	heat-transfer correlation constant
k	total thermal conductivity (including the chemical reaction terms)
$\lambda$	$\frac{\rho\mu}{\rho_w\mu_w}$
Nu	Nusselt number, $\frac{\dot{q}c_{p_w}x}{(H_e - H_w)k_w}$
n	exponent, 0 for two-dimensional flow and 1 for three-dimensional flow
p	pressure
$\dot{q}$	heat-transfer rate

R	gas constant
$R_e$	Reynolds number, $\frac{\rho_e u_e x}{\mu_e}$
$R_w$	Reynolds number, $\frac{\rho_w u_e x}{\mu_w}$
r	radius of cross section
St	Stanton number, $\frac{\dot{q}}{(H_e - H_w)\rho_e u_e}$
T	temperature
u,v	components of velocity in x and y directions
x,y	coordinates along a body meridian and normal to a body generator
$\beta$	pressure gradient parameter (see eq. (9))
$\delta$	boundary-layer thickness to $\frac{u}{u_e} = 0.995$
$\delta^*$	boundary-layer displacement thickness
$\Phi, \Phi_1, \Phi_2, \Phi_3, \Phi_4$	convergence criteria (see eqs. (15), (16), (17), and (18))
$\rho$	air density
$\theta$	boundary-layer momentum thickness
$\theta_c$	cone half-angle
$\mu$	coefficient of viscosity
$\tau$	shear stress
$\eta, \zeta$	transformed coordinates defined by equation (7)
$\sigma$	total Prandtl number, $\mu \frac{c_p}{k}$

#### Subscripts

b	at model base
e	conditions at edge of boundary layer
i	number of iteration

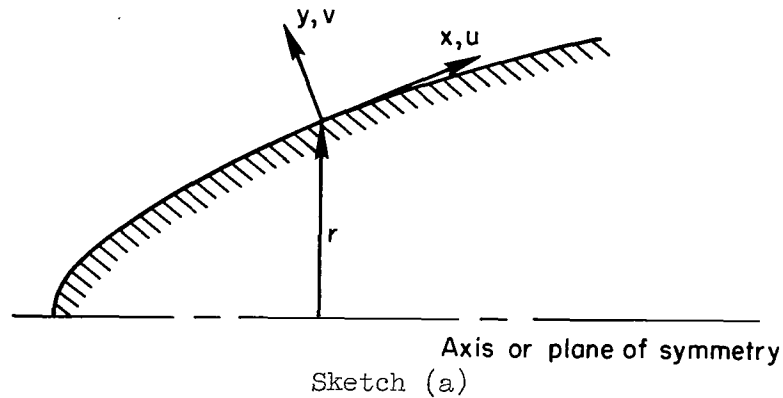
st      stagnation conditions  
w      wall conditions  
 $\eta, \zeta$       differentiation with respect to  
 $\infty$       free-stream conditions

## ANALYSIS

The boundary-layer equations and the initial steps in their solution are first stated in general terms in order to illustrate a wider application of the method of solution. Subsequently, the simplifications pertinent to flow over isothermal cones are made.

### General Equations

The general equations for a thin laminar boundary layer for a dissociating and ionizing gas in equilibrium are, in the Coordinate System defined by sketch (a), the continuity equation



$$\frac{\partial(\rho u r^n)}{\partial x} + \frac{\partial(\rho v r^n)}{\partial y} = 0 \quad (1)$$

the momentum equation

$$\rho u \frac{\partial u}{\partial x} + \rho v \frac{\partial u}{\partial y} = - \frac{\partial p}{\partial x} + \frac{\partial[\mu(\partial u / \partial y)]}{\partial y} \quad (2)$$

and the energy equation

$$\rho u \frac{\partial h}{\partial x} + \rho v \frac{\partial h}{\partial y} = u \frac{\partial p}{\partial x} + \mu \left( \frac{\partial u}{\partial y} \right)^2 + \frac{\partial \left( \frac{k}{c_p} \frac{\partial h}{\partial y} \right)}{\partial y} \quad (3)$$

The gas state and transport properties  $c_p$ ,  $k$ , and  $\mu$  include the chemical reaction terms implicitly (i.e., they are total properties as defined by Hansen, ref. 8). The exponent  $n$  in equation (1) is 0 for two-dimensional flow and 1 for axially symmetric flow. Equations (1), (2), and (3) are based on the usual thin boundary-layer assumptions. Energy transport by radiation has been neglected. The neglect of radiative transport is realistic if the ratio of the energy radiated (per unit mass along a stream line) to the local static enthalpy is small. The range of applicability of this assumption is hard to define because this ratio depends on the free-stream velocity, cone angle, and the distance along the stream line, and will for the case of a small angle cone have its maximum within the boundary layer. For this case the neglect of energy transport by radiation is conservative in that the convective heat-transfer rates thus calculated are on the high side. The pressure gradient term has been retained for generality but will be set equal to zero for the cone solutions.

By letting

$$H = h + \frac{u^2}{2} \quad (4)$$

and combining equation (2) with equation (3), we obtain

$$\rho u \frac{\partial H}{\partial x} + \rho v \frac{\partial H}{\partial y} = \frac{\partial \left( \frac{\mu}{\sigma} \frac{\partial H}{\partial y} \right)}{\partial y} + \frac{\partial \left[ \frac{\mu}{2} \left( 1 - \frac{1}{\sigma} \right) \left( \frac{\partial u^2}{\partial y} \right) \right]}{\partial y} \quad (5)$$

where  $\sigma$  is the Prandtl number.

The solution of the boundary-layer problem with zero mass injection requires solving equations (1), (2), and (5) simultaneously for boundary conditions

at  $y = 0$

$$u = v = 0 \text{ and } H = H_w$$

and as  $y \rightarrow \infty$

$$u \rightarrow u_e \text{ and } H \rightarrow H_e$$

} (6)

Equations (1), (2), and (5) may be put into a form more suitable for solution by use of the Howarth and Mangler transformations

$$\eta \equiv \frac{r^n u_e}{\sqrt{2\xi}} \int_0^y \rho \, dy \quad (7)$$

$$\zeta \equiv \int_0^x \rho_w \mu_w u e^{r^{2n}} dx$$

and the following dimensionless dependent variables

$$f_\eta = \frac{u}{u_e}, \quad f = \int_0^\eta f_\eta d\eta, \quad \text{and} \quad g = \frac{H}{H_e} \quad (8)$$

Substituting equations (1), (7), and (8) into equations (2) and (5) yields

$$(zf_\eta)_\eta + ff_\eta + 2\beta\left(\frac{\rho_e}{\rho} - f_\eta^2\right) = 2\zeta(f_\eta f_\eta \zeta - f_\zeta f_\eta \eta) \quad (9)$$

and

$$\left(\frac{l}{\sigma} g_\eta\right)_\eta + fg_\eta + \frac{u_e^2}{H_e} \left[ \left(1 - \frac{l}{\sigma}\right) zf_\eta f_\eta \eta \right] = 2\zeta(f_\eta g_\eta \zeta - f_\zeta g_\eta) \quad (10)$$

where

$$l = \rho\mu/\rho_w\mu_w$$

and

$$\beta = \frac{d}{d \ln \zeta} \ln \frac{u_e}{\rho_e}$$

The boundary conditions transform to

at  $\eta = 0$

$$f = f_\eta = 0 \quad g = g_w$$

and as  $\eta \rightarrow \infty$

$$f_\eta \rightarrow 1 \quad g \rightarrow 1$$

(11)

Gas properties.— The solution of equations (9) and (10) requires an equation of state and equations for the transport properties. As these properties are allowed to vary, they can form an important part of the analysis. The equation of state for air in equilibrium can be written

$$\rho = \rho(h,p) \quad (12)$$

The transport properties are the total properties as defined by Hansen (ref. 9). Inspection of equations (9) and (10) reveals that the gas properties occur in discrete, select groupings - that is,  $\rho$ ,  $\rho\mu$ , and  $\rho\mu/\sigma$ . These

groupings have been correlated by Viegas and Howe (ref. 10) as functions of the static enthalpy,  $h$ , and the pressure,  $p$ , for equilibrium air. The correlations were fitted with analytical curves by Viegas and Howe for use on electronic digital computers. These curve fits were used to obtain the solutions presented in the present report. Because the correlation curves of Viegas and Howe do not apply at temperatures below  $1000^{\circ}$  K, "perfect gas" relationships were used for temperatures below  $1000^{\circ}$  K. The "perfect gas" relations were modified slightly to remove any discontinuity in properties at  $1000^{\circ}$  K.

### Solution of Equations

Equations (9) and (10) are general for equilibrium flow except for the usual assumptions of a thin boundary layer and the disregard of radiative transport; but because the right sides of the equations are not similar, they are very difficult to solve and must be solved at many points along a given body shape. However, for a cone or a flat plate with isothermal wall, derivatives with respect to  $\zeta$  are identically zero because neither the boundary conditions nor the flow properties vary in the  $\zeta$  direction (i.e., the solutions are similar). Making use of this fact and setting  $\beta = 0$  we simplify equations (9) and (10) to

$$(\lambda f_{\eta\eta})_{\eta} + f f_{\eta\eta} = 0 \quad (13)$$

$$\left(\frac{\lambda}{\sigma} g_{\eta}\right)_{\eta} + f g_{\eta} + \frac{u_e^2}{H_e} \left[ \left(1 - \frac{1}{\sigma}\right) \lambda f_{\eta} f_{\eta\eta} \right]_{\eta} = 0 \quad (14)$$

Equations (13) and (14) are coupled through the transport properties, state properties, and the function  $f$  and its derivatives. The coupling between the momentum equation and the energy equation for boundary-layer flow has been demonstrated to be weak or known under certain conditions. For example, reasonable stagnation-point heat-transfer rates (i.e., for  $\beta \neq 0$ ) were calculated by Lees (ref. 11) assuming the value of  $\lambda$  to be unity. Also for  $\sigma$  equal to unity the Crocco equation relates equations (13) and (14) directly. This weak coupling and the Crocco equation have been used to obtain rapid solutions in the following manner.

Assume a solution for equation (14). Equation (13) can then be considered as a third-order ordinary differential equation with known variable coefficients and its solution for given boundary conditions may be obtained readily (see next section for procedure used in solving the differential equations). Similarly, equation (14) can be solved for an assumed solution of equation (13). Therefore, if an approximate solution to one of the equations is known, the exact solution may be obtained by iteration between the two equations. This process continues until the solutions converge; that is,

$$|f_i - f_{i-1}| = \varphi_1 \quad (15)$$

and

$$|g_i - g_{i-1}| = \varphi_2 \quad (16)$$

where  $\varphi_1$  and  $\varphi_2$  are required to approach zero with increasing number of iterations,  $i$ . Since it is impractical to check the functions  $f$  and  $g$  at many points, the derivatives of  $f$  and  $g$  were checked at the wall; that is,

$$\left| f_{\eta\eta_{w_i}} - f_{\eta\eta_{w_{i-1}}} \right| = \varphi_3 \quad \begin{array}{l} \varphi_3 \rightarrow 0 \\ i \rightarrow \infty \end{array} \quad (17)$$

and

$$\left| g_{\eta_{w_i}} - g_{\eta_{w_{i-1}}} \right| = \varphi_4 \quad \begin{array}{l} \varphi_4 \rightarrow 0 \\ i \rightarrow \infty \end{array} \quad (18)$$

Because of the nonlinearities involved, this cannot be proved to be an absolutely convergent procedure, nor can it be shown to be unique. However, in cases where the solutions have been compared with those obtained by other investigators using other procedures, the agreement is very good.

There is still the problem of how to get the first approximate solution to start the iteration procedure. Consider equation (13); note that the only term which depends on equation (14) is the ratio  $\rho\mu/\rho_w\mu_w$ . This is a function of the static enthalpy

$$\frac{\rho\mu}{\rho_w\mu_w} = \frac{\rho\mu}{\rho_w\mu_w} (h)$$

where  $h$  may be written as a function of  $g$  and the first derivative of  $f$  as

$$h = H_e g - \frac{u_e^2}{2} f_{\eta}^2 \quad (19)$$

Now by the use of the Crocco equation (ref. 12)

$$g = (1 - g_w) f_{\eta} + g_w \quad (20)$$

$h$  can be expressed as

$$h = H_e(1 - g_w) f_{\eta} + H_e g_w + \frac{u_e^2}{2} f_{\eta}^2 \quad (21)$$

Equation (13) can now be solved independently of equation (14).

The process outlined above provides for very rapid convergence. A typical example of the convergence process is given in appendix A.

Numerical analysis procedures employed.- Each of equations (13) and (14) was solved by integration, using a fourth-order Adams-Moulton method (ref. 13) with variable step size and double precision arithmetic to minimize round-off errors. The procedure was to select an initial value of  $f_{\eta\eta}$  or  $g_{\eta}$  at the

wall and integrate until  $\eta$  became large, or some other condition such as  $f_{\eta\eta}$  or  $g_{\eta}$  asymptotically approached zero or  $f_{\eta}$  or  $g$  became excessively large. In any case a second value of  $f_{\eta\eta}$  or  $g_{\eta}$  was determined and the equation integrated again. This was repeated three times and the results linearly extrapolated to the outer boundary condition to obtain a fourth value. This procedure was repeated with smaller and smaller changes in the initial value until the solution had converged within prescribed limits. The limits prescribed for the results presented in this paper are

$$\begin{array}{ll} f_{\eta} \text{ and } g \text{ at large } \eta & 1.0 \pm 0.001 \\ f_{\eta\eta} \text{ and } g_{\eta} \text{ at large } \eta & 0 \pm 0.001 \\ f_{\eta\eta} \text{ and } g_{\eta} \text{ at } \eta = 0 & \pm 0.001 \end{array}$$

These limits were found to give results which were accurate within  $\pm 1/2$  percent. Large changes in these limits were found to have only a very small effect on the final results. See appendix A for more details on the effects of various quantities on the convergence.

#### Heat-Transfer, Skin-Friction, and Boundary-Layer-Thickness Parameters

The methods used to calculate heat transfer, skin friction, and various boundary-layer thicknesses from the solutions of equations (13) and (14) are outlined in the following paragraphs.

Heat transfer.- The heat transfer to a surface in equilibrium air in the absence of radiation is

$$\dot{q} = k_w \left. \frac{\partial T}{\partial y} \right|_w \quad (22)$$

When the transformations in equation (7), and the dimensionless variables (eq. (8)) are applied, equation (22) becomes

$$\dot{q} = \frac{k_w H e r^n u_e \rho_w}{c_{p_w} \sqrt{2\zeta}} g_{\eta_w} \quad (23)$$

This equation is general and can be used for either two- or three-dimensional flow and can be applied downstream of a slightly blunted nose or leading edge, if similarity is assumed to hold and  $\beta = 0$ . However, for the present purpose we consider only the case of a sharp cone with an isothermal wall. For this case  $\mu_w$ ,  $\rho_w$ , and  $u_e$  are constant and the radius of cross section is given as  $r = x \sin \theta_c$ , where  $\theta_c$  is the cone half-angle. With this restriction equation (23) may be written as

$$\dot{q} = \frac{\sqrt{R_w} k_w H_e \sqrt{3/2}}{c_{p_w} x} g_{\eta_w} \quad (24)$$

where

$$R_w = \frac{\rho_w u_e x}{\mu_w}$$

This may be rearranged to form the Nusselt number, Nu, divided by the square root of the Reynolds number,  $R_w$ ,

$$\frac{Nu}{\sqrt{R_w}} = \frac{\dot{q} c_{p_w} x}{(H_e - H_w) k_w \sqrt{R_w}} = \sqrt{\frac{3}{2}} \frac{g_{\eta_w}}{1 - g_w} \quad (25)$$

All of the heat-transfer results presented herein are in this form.

Skin friction.— The local shear stress,  $\tau$ , on the wall can be expressed as

$$\tau = \mu_w \left. \frac{\partial u}{\partial y} \right|_w \quad (26)$$

When the transformations and dimensionless forms in equations (7) and (8) are applied, this becomes

$$\tau = \frac{\mu_w u_e^2 r^n \rho_w}{\sqrt{2\zeta}} f_{\eta_w} \quad (27)$$

This equation is general in the same sense that equation (23) is for heat transfer. However, for the purpose of this paper we will again consider only the case of a sharp cone with isothermal wall. If properties consistent with such restrictions are used, and the shear stress is divided by the local dynamic pressure  $[(1/2) \rho_e u_e^2]$ , the local skin-friction coefficient,  $c_f$ , can be written as

$$c_f = \frac{\sqrt{6} f_{\eta_w}}{\sqrt{Re} \sqrt{l_e}} \quad (28)$$

or

$$c_f \sqrt{Re} = \frac{\sqrt{6} f_{\eta_w}}{\sqrt{l_e}} \quad (29)$$

where

$$Re = \rho_e u_e x / \mu_e$$

and

$$\lambda_e = \rho_e \mu_e / \rho_w \mu_w$$

Note that different Reynolds numbers are used for heat transfer and skin friction to simplify the correlations.

If we now integrate the local skin friction over the length of the cone and divide by the surface area, we obtain an average skin-friction coefficient as

$$C_F \sqrt{Re_{x_b}} = \frac{\frac{4}{3} \sqrt{6} f_{\eta} \eta_w}{\sqrt{\lambda_e}} \quad (30)$$

where

$$Re_{x_b} = \frac{\rho_e u_e x_b}{\mu_e}$$

Boundary-layer-thickness parameters.— There are several thickness parameters associated with boundary layers. The three most commonly used are the boundary-layer thickness,  $\delta$ , defined as the distance,  $y$ , at which the boundary-layer-flow velocity has reached  $0.995 u_e$ ; the displacement thickness,  $\delta^*$ , defined as

$$\delta^* = \int_0^{y(u/u_e = 0.995)} \left(1 - \frac{\rho}{\rho_e} f_{\eta}\right) dy \quad (31)$$

and the momentum thickness,  $\theta$ , defined as

$$\theta = \int_0^{y(u/u_e = 0.995)} \frac{\rho}{\rho_e} f_{\eta} (1 - f_{\eta}) dy \quad (32)$$

These thicknesses for the case of cone flow, appropriately made dimensionless, were calculated by applying the transformations and dimensionless forms described earlier, as follows

$$\frac{\delta \sqrt{Re}}{x} = \sqrt{\frac{2}{3\lambda_e}} \int_0^{\eta_e} \frac{\rho_e}{\rho} d\eta \quad (33)$$

and

$$\frac{\delta^* \sqrt{Re}}{x} = \sqrt{\frac{2}{3\lambda_e}} \int_0^{\eta_e} \left(\frac{\rho_e}{\rho} - f_{\eta}\right) d\eta \quad (34)$$

and

$$\frac{\theta \sqrt{Re}}{x} = \sqrt{\frac{2}{3\lambda_e}} \int_0^{\eta_e} f_\eta (1 - f_\eta) d\eta \quad (35)$$

where  $\eta_e$  is the value of  $\eta$  at which  $f_\eta = u/u_e = 0.995$ .

The integrations indicated in equations (33), (34), and (35) were performed by use of the Simpson rule.

Additional heat-transfer, skin-friction, and boundary-layer-thickness parameters are listed in appendix B, as well as formulas for conversion from one form to another. All of the foregoing discussion on heat-transfer, skin-friction, and boundary-layer-thickness parameters is applicable to a flat plate merely by striking out the 3's wherever they occur.

## RESULTS AND DISCUSSION

Equations (13) and (14) were solved for the following range of conditions:

$u_\infty$	3.05 to 24.4 km/sec
$u_e^2/2H_e$	0 to 0.93
$p_e$	0.1 to 10 atm
$T_w$	1000° to 4200° K

Solutions for the lower values of  $u_\infty$ , less than 10 km/sec, were used to check the present solutions against others which included only dissociation effects. The upper limit was dictated by the maximum temperature for which the thermodynamic and transport properties of air are available.

The parameter  $u_e^2/2H_e$  can be interpreted as a cone-angle parameter. Using impact theory for a cone (i.e.,  $u_e = u_\infty \cos \theta_c$ ) and neglecting the small contribution of the free-stream static enthalpy to the total enthalpy, one can express this parameter as

$$u_e^2/2H_e = \cos^2 \theta_c \quad (36)$$

where  $\theta_c$  is the cone half-angle. (This must be modified for cones with small amounts of bluntness, but at the speeds of interest this modification is small.) By use of this relationship, values of  $u_e^2/2H_e$  of 0, 0.25, 0.50, 0.75, and 0.93 correspond to cone half-angles of 90°, 60°, 45°, 30°, and 15°, respectively. For the 90° cone, the shock wave will be detached and the assumption of conical flow will not apply. However, a different interpretation can be placed on the parameter in this case, since  $u_e^2/2H_e = 0$

also corresponds to solutions for zero Mach number with zero pressure gradient and very high free-stream static enthalpy. Such a condition may represent flow in the heat exchangers of a reactor, for example.

Most of the solutions were obtained for a boundary-layer pressure of 1 atmosphere. A few solutions were obtained at pressures of 0.1 and 10 atmospheres to assess the effect of pressure.

The wall temperatures were chosen to cover the range of probable interest for entry vehicles.

### Velocity and Enthalpy Profiles

Typical examples of solutions to equations (13) and (14) are tabulated in table I. The variables of primary interest,  $u/u_e$ ,  $H/H_e$ , and  $h/h_e$  are also plotted in figure 1 as functions of the dimensionless distance normal to the surface,  $\eta$ , for two cases. The velocity profiles are shown in figure 1(a). These profiles are similar to those obtained by Van Driest (ref. 14). The inflections exhibited by these curves result from transformation from  $y$  to  $\eta$  and do not exist when plotted in the physical coordinates. A numerical inverse transformation was performed to verify this but it is too cumbersome to present here.

The total-enthalpy profiles shown in figure 1(b) are similar to those of reference 14. There is a slight overshoot in  $H/H_e$  (i.e.,  $g$  exceeds 1) near the outer edge of the boundary layer for the larger values of  $u_e^2/2H_e$  (difficult to detect at the scale plotted). This overshoot is a result of a Prandtl number less than unity and the maximum temperature occurring near the center of the boundary layer.

The static-enthalpy profiles are shown in figure 1(c). These profiles are indicative of the temperature profiles. Note that, as stated above, the maximum static enthalpy, or temperature, occurs near the center of the boundary layer for  $u_e^2/2H_e$  greater than about 0.5. These profiles are very similar to the temperature profiles of reference 14. Although it can not be detected in these figures, it is evident in table I that at the edge of the boundary layer, the static enthalpy has not returned entirely to the edge values for large  $u_e^2/2H_e$ . This discrepancy is a result of the convergence criteria placed on  $u/u_e$  and  $H/H_e$ , which have to be combined to yield  $h/h_e$ . This does not, however, have any appreciable influence on the skin-friction, heat-transfer, or boundary-layer-thickness results.

### Comparison With the Crocco Equation

The similarity of solutions of the momentum and energy equations for a Prandtl number of unity was first shown by L. Crocco for a perfect gas in

reference 12. The generalization of his result to a real gas in chemical and thermodynamic equilibrium follows in a similar fashion to yield equation (20).

A comparison of this result (eq. (20)) to the calculation for variable Prandtl number, the present solutions, is shown in figure 2. The close agreement probably accounts for the very rapid convergence of the calculation procedure employed, which uses the Crocco equation to help calculate the state properties and transport properties for the first approximate solution to the momentum equation.

A commonly used way of extending the Crocco equation is to differentiate equation (20) with respect to the independent variable  $\eta$  to yield

$$g_{\eta} = (1 - g_w)f_{\eta\eta} \quad (37)$$

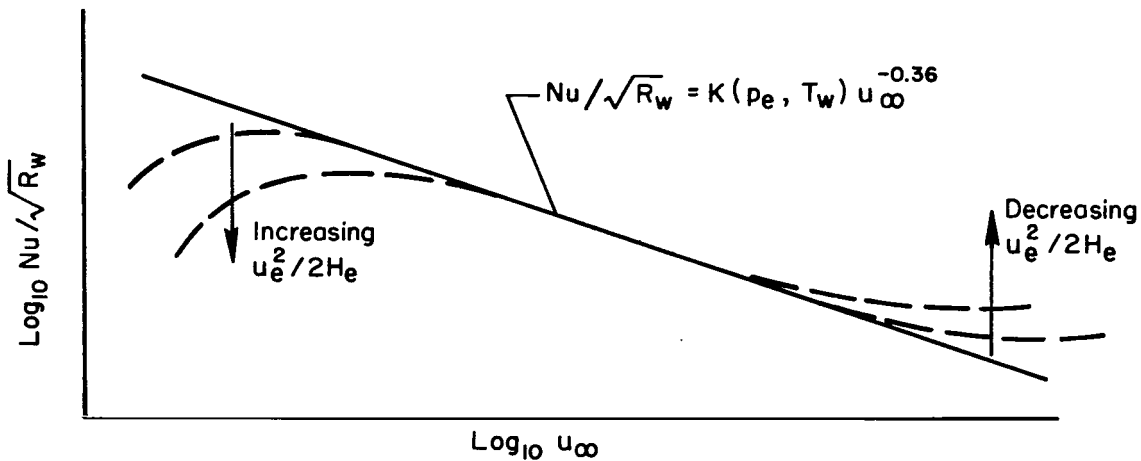
This equation provides a simple relationship between heat transfer and skin friction. However, it is not accurate for the present conditions, as can be seen from an examination of the initial slopes of the curves in figure 2. From analogy, this would imply that Reynolds analogy is questionable under these conditions. This was also noted in reference 8.

#### Presentation and Correlation of Heat-Transfer Results

The heat-transfer, skin-friction, and three boundary-layer-thickness parameters obtained from the solutions are listed in table II. Other information essential to devising correlations of these results is included. The effects of flow conditions and wall temperature on these results are discussed in the following paragraphs. Comparisons are made with other theoretical results where available.

The heat-transfer results are shown in figure 3 in the form  $Nu/\sqrt{R_w}$  as a function of velocity  $u_{\infty}$ . The data in this form are easy to use, since the flow properties are evaluated at the wall where the effects of dissociation and ionization are least strong. The results are also correlated by this type of presentation.

Correlation.- The general features of the correlation plots (fig. 3) are shown in sketch (b). Most of the present solutions were correlated by the straight line,  $Nu/\sqrt{R_w} = K(p_e, T_w)u_{\infty}^{-0.36}$ . Deviations from the correlation were noted with high wall temperature at low velocities and to a somewhat smaller extent with large cone angles at high velocities, as indicated by the dashed lines in sketch (b). The reasons for these deviations will be discussed.



Sketch (b)

Plotted in the manner of sketch (b), the results are independent of the parameter  $u_e^2/2H_e$  (i.e., cone angle), except as noted.

The effects of the wall temperature and pressure on the correlation enter through the parameter  $K(p_e, T_w)$ , as illustrated in figure 4. Particularly at pressures above 1 atmosphere, the effect of pressure change is small compared to the effect of wall temperature change. This insensitivity to pressure above 1 atmosphere is a result of the small effect of pressure on the thermodynamic and transport properties, as may be observed in reference 10. In most cases of practical interest and at pressures of less than 1 atmosphere the effects of nonequilibrium have to be considered, thereby introducing additional complications not considered herein. It is thought that for most calculations the correlation parameter for a pressure of 1 atmosphere will give satisfactory results; this may be approximated by the equation  $K(p_e, T_w) = 0.280 T_w^{+0.1335}$ , where the constant 0.280 has units of  $(\text{km}/\text{sec})^{0.36} \text{ } ^\circ\text{K}^{-0.1335}$ .

Deviations from the correlation.- There are two conditions under which significant deviations from the correlation curves occur. The first of these is when the wall enthalpy approaches the recovery enthalpy. This condition is characterized by low  $u_\infty$  and large  $u_e^2/2H_e$  and is indicated by the dashed lines on the left side of sketch (b). This deviation is a result of using the difference between stagnation enthalpy and wall enthalpy rather than the difference between recovery enthalpy and wall enthalpy in defining the Nusselt number. However, because of the simplicity of determining the stagnation enthalpy and the difficulties encountered in determining the recovering enthalpy, it was thought that the use of the stagnation enthalpy was more practical.

The second condition under which deviations occur is when the air in the outer portion of the boundary layer becomes highly ionized. This happens only at speeds greater than 9 to 10 km/sec and appears to be a strong function of

the parameter,  $u_e^2/2H_e$ , and pressure. The effect of the cone-angle parameter results from its effect on the static temperature and thus on the degree of ionization; decreasing  $u_e^2/2H_e$  (i.e., increasing cone angle), increases the static temperatures and thus increases the degree of ionization. This effect can be seen in figure 3(a). The effect of pressure on this deviation from the correlation is one of changing the degree of ionization and may be seen by comparing figures 3(b), 3(d), and 3(e). No appreciable effect of wall temperature on deviations due to ionization is evident, probably because the wall temperatures considered are relatively small in comparison to ionization temperatures.

Comparison with other theoretical results.- The present results were compared with those of references 7 and 8. For the purpose of comparison with the results of reference 7 the logarithm of  $Nu/\sqrt{R_w}$  was plotted in figure 5(a) versus the logarithm of  $(\rho_e \mu_e / \rho_w \mu_w)_{st}$  (the subscript st indicates that the ratio is evaluated at the stagnation condition behind a normal shock at the flight conditions in question.) The agreement of the present results with the correlation curve of reference 7 is very good until ionization begins. At this point discrepancies between the present results and the extrapolated results of reference 7 appear and become very large with increasing velocity. At a speed of 15 km/sec the present results are larger by a factor of 1.50 than the extrapolated results of reference 7.

A comparison with the theoretical results of reference 8 is shown in figure 5(b). There the solid lines are the present correlation curves and the circles are results from reference 8. Note that for velocities of 4.36 and 6.23 km/sec there is generally good agreement between the results. The agreement at 10.86 km/sec, however, is poor. This is probably a result of the transport properties used; in these particular results the calculated transport properties used (ref. 8) did not include the effects of ionization.

Calculation of heat transfer to a cone.- Up to this point the heat-transfer results have been presented in the form  $Nu/\sqrt{R_w}$ , with all flow variables evaluated at either wall conditions or boundary-layer edge conditions. This form permits the results to be presented without restriction as to the solution of the inviscid cone-flow problem. In order to apply these results to a heat-transfer calculation, it is necessary to make some assumptions about the inviscid cone flow. We will assume that all of the flow variables at the boundary-layer edge may be calculated by simple modified impact relations, where the pressure relationship is

$$\frac{p_e}{p_\infty} = \frac{\frac{1}{2} c_{p_{max}} \rho_\infty u_\infty^2 \sin^2 \theta_c + p_\infty}{p_\infty} \quad (38)$$

and the velocity relationship is

$$u_e = u_\infty \cos \theta_c \quad (39)$$

where  $c_{pmax}$  is the stagnation-point pressure coefficient;  $c_{pmax}$  is between 1.8 and 1.9 for most cases. Using these relationships and the correlation equation shown in sketch (b), we can write the local heat-transfer rate as

$$\dot{q} = \frac{K(p_e, T_w) \sqrt{P_w \mu_w}}{\sigma_w} \sqrt{\frac{\cos \theta_c}{x}} u_\infty^{0.14} (H_e - H_w) \quad (40)$$

If we now use an equation of state of the form

$$\rho = p/zRT \quad (41)$$

and note that, for the wall temperatures and pressures considered, the compressibility factor  $z$  differs only slightly from 1 (we will therefore assume it to be identically 1), that  $H_e \gg H_w$  and that  $p_e \gg p_\infty$ , we can rewrite equation (40), using the expression  $K(T_w, p_e) = 0.280 T_w^{0.1335}$ , as

$$\dot{q} = \frac{1}{2} \left( \frac{0.268 T_w^{0.1335}}{\sigma_w} \sqrt{\frac{\mu_w}{RT_w}} \right) \left( \sqrt{\rho_\infty} \right) \left( \frac{\sin \theta_c}{x} \sqrt{\frac{\cos \theta_c}{x}} \right) \left( u_\infty^{3.14} \right) \quad (42)$$

where the constant 0.268 has the units  $(\text{km/sec})^{0.36} \text{ } ^\circ\text{K}^{-0.1335}$ . The terms in the first parentheses represent the dependence on wall temperature (the effect of pressure being very small on any of these terms). This group of terms is nearly constant, varying only a few percent for wall temperatures from  $1000^\circ$  to  $4200^\circ$  K. The term in the second set of parentheses is the altitude dependence; the third group, the geometry dependence; and the last group, the velocity dependence.

In practice, the tips of the cones will generally be blunt either by design or as a result of ablation. The influence of small amounts of tip blunting on the skin friction and heat transfer is considered in appendix C.

#### Presentation and Correlation of Skin-Friction Results

Typical skin-friction results are shown in figure 6. Formulas for conversions to other parametric forms are given in appendix B.

Correlation.— The skin-friction results were not so readily correlated as the heat-transfer results. A useful correlation was obtained when the parameter  $c_f \sqrt{Re}$  was plotted versus  $u_e^2/2H_e$  as shown in figure 6. Note that  $c_f \sqrt{Re}$  decreases with increasing  $u_e^2/2H_e$  (i.e., with decreasing cone angle). The equation of the correlation curves shown, which fits the results fairly well in most cases, is

$$c_f \sqrt{Re} = a - b(u_e^2/2H_e)^m \quad (43)$$

where  $a$  is a function of the wall temperature as shown in figure 7,  $b$  is a constant equal to 0.506, and  $m$  is a constant equal to 2.2. This simple correlation curve represents the calculated values within  $\pm 10$  percent in most cases.

Deviations from the correlation.- The main deviations from the correlation curve (fig. 6) occur at the same conditions at which deviations from the heat-transfer correlation occur, namely, (1) near-zero heat transfer and (2) when a large fraction of the outer part of the boundary layer becomes appreciably ionized. The first of these effects is evident in figure 6(b). Here the wall enthalpy has become a large fraction of the stagnation enthalpy (i.e., nearing zero heat transfer) for the 4.56 km/sec results, causing them to deviate from the 9.12 km/sec results; this is also evident in results for higher wall temperatures.

The effect of ionization is evident to some degree at all wall temperatures and pressures considered. It results in an increase in the skin-friction parameter with decreasing  $u_e^2/2H_e$  for the higher speeds - that is, higher total enthalpies. Also the lower pressure results are not so well correlated as the higher pressure results, an effect which is again attributable to ionization.

Comparison with other theoretical results.- Comparison with the theoretical perfect-gas results of Van Driest (ref. 14) is shown in figure 8(a). The curve from reference 14 is for a ratio of  $T_w/T_e$  (or  $h_w/h_e$ ) of 0.25. The present results agree fairly well with those of reference 14. The slight increase in the skin-friction parameter for the present results is attributable to real-gas effects. The discrepancy is greater at the smaller values of  $u_e^2/2H_e$  because of higher temperatures in the boundary layer. The inflection in the skin-friction curve near  $u_e^2/2H_e$  equal to zero is probably an effect of the beginning of ionization.

Comparison with the results of reference 8 and the "reference enthalpy" method of reference 15 is shown in figure 8(b). The present results agree well with both of these sets of results for nearly the entire range of conditions considered in the present report. The exception was for conditions when the boundary-layer air was appreciably ionized.

It would appear that the reference enthalpy method would predict skin friction more accurately than the present correlation equation, but would probably be more difficult to apply.

Calculation of the friction drag coefficient on a cone.- The skin-friction drag coefficient, based on the base area, is obtained when the local skin friction is integrated over the cone as follows:

$$C_{Df} = \frac{2 \sin \theta_c \cos \theta_c}{r_b^2 \rho_\infty u_\infty^2} \int_0^{x_b} \frac{(c_{f\sqrt{Re}}) \rho_e u^2 x_e}{\sqrt{Re}} dx \quad (44)$$

Substituting equation (39) into equation (44) yields

$$C_{Df} = \frac{2 \sin \theta_c \cos^3 \theta_c}{r_b^2} \frac{\rho_e}{\rho_\infty} \int_0^{x_b} (c_f \sqrt{Re}) \frac{x}{\sqrt{Re}} dx \quad (45)$$

Now using the correlation equation for the skin-friction parameter and equation (36), integrating and rearranging, we obtain

$$C_{Df} = \frac{4}{3} \frac{\cos^{5/2} \theta_c}{\sin \theta_c} \frac{(a - 0.506 \cos^{4.4} \theta_c)}{\sqrt{R_\infty x_b}} \sqrt{\frac{\rho_e \mu_e}{\rho_\infty \mu_\infty}} \quad (46)$$

where

$$R_\infty x_b = \frac{\rho_\infty u_\infty x_b}{\mu_\infty}$$

It is very difficult to ascertain the separate effects of various conditions on  $C_{Df}$  because of the dependence of  $\rho_e \mu_e$  on both the free-stream velocity and the cone angle.

Some general effects of small amounts of bluntness are discussed briefly in appendix C.

### Boundary-Layer-Thickness Parameters

Three boundary-layer-thickness parameters, the boundary-layer thickness  $\delta$ , the displacement thickness  $\delta^*$ , and the momentum thickness  $\theta$ , made dimensionless by  $(1/x)\sqrt{Re}$ , were calculated for various values of  $u_e^2/2H_e$ .

Boundary-layer thickness.— The boundary-layer thickness out to  $u/u_e = 0.995$  is shown in figure 9. For a given local Reynolds number the boundary layer increases in thickness with increasing  $u_e^2/2H_e$  (i.e., decreasing cone angle). This general trend holds for all velocities, wall temperatures, and pressure levels considered. The effect of pressure level was small. The effects of wall temperature and free-stream velocity on the boundary-layer thickness appear to be closely related and their combined effect appears to correlate with  $g_w$  (i.e.,  $2h_w/u_\infty^2$ ). This is shown in figure 10. Here some typical values for a dimensionless boundary-layer thickness are plotted versus  $g_w$ . Except for some scatter at small values of  $g_w$ , increasing  $g_w$  increases the boundary-layer thickness.

The effect of ionization appears to be one of thickening the boundary layer; this occurs at high speeds and for small values of  $u_e^2/2H_e$ . Note in figure 9 the boundary-layer thickness for 15.20 km/sec increases with decreasing  $u_e^2/2H_e$  below  $u_e^2/2H_e = 0.5$ .

A brief comparison of the boundary-layer thickness with the theoretical results of reference 14 is shown in figure 9. The curve from reference 14 is for a ratio of  $h_w/h_e$  of 0.25. No attempt at putting the present results into a constant  $h_w/h_e$  form was made because of the small variations in the boundary-layer thickness with the various parameters. The agreement between the results of reference 14 and the present results is good. The agreement would be better if the effect of changing  $h_w/h_e$  were considered.

Displacement thickness.- Typical results of boundary-layer displacement thickness are plotted versus  $u_e^2/2H_e$  in figure 11. The general trends of the results, with the various parameters  $u_e^2/2H_e$ ,  $T_w$ ,  $u_\infty$ , and  $p_e$  are very similar to those exhibited by the boundary-layer thickness, except the effect of ionization is not noticeable on the displacement thickness. There is one very interesting fact evident in this figure - that is, the displacement thickness appears to get very small and possibly take on even negative values for small values of the parameter  $u_e^2/2H_e$  when the value of  $g_w$  is very small. This phenomenon may be of interest in the design of high-speed inlet systems or forced gas heat exchangers in nuclear reactors. Under these conditions the mass flow through the system might be larger than one would expect.

Momentum thickness.- Typical results for boundary-layer momentum thickness are plotted in the same manner as the other boundary-layer thicknesses in figure 12. The general trends exhibited by these results are very similar to the trends exhibited by the skin-friction results. The reason for this similarity is that the momentum thickness is, by definition, proportional to a momentum defect (or loss) from the main flow over the cone. This loss has to appear as drag to the surface over which the boundary layer flows. This fact has been used for years in subsonic wind tunnels to determine drag.

## SUMMARY OF RESULTS

The boundary-layer equations in axisymmetric flow with zero pressure gradient for air in chemical and thermodynamic equilibrium have been solved for a wide range of conditions. From these solutions the heat transfer, skin friction, boundary-layer thickness, displacement thickness, and momentum thickness for cones in hypervelocity flight have been computed. The following are some of the results of these calculations.

Good correlation of the heat-transfer results was obtained when the Nusselt number divided by the square root of the Reynolds number,  $R_w$ , was plotted versus the free-stream velocity. The effect of the cone-angle parameter on this correlation was negligible. The effects of wall temperature and pressure level were accounted for in the correlation. Two regions of poor correlation were noted, one near zero heat transfer and the other at conditions where the degree of ionization was very high. The present results indicate heat-transfer rates which are higher than extrapolations of earlier theoretical results which include only dissociation and neglect ionization.

A fair correlation was found for the skin-friction results. This correlation allows for the simple estimation of the friction drag. A better method for calculating skin friction is the reference enthalpy method; however, it is somewhat more difficult to use. There were no major effects of dissociation and only small amounts of ionization on the skin-friction parameter,  $c_f\sqrt{Re}$ . However, large amounts of ionization tend to increase the value of  $c_f\sqrt{Re}$ .

No attempt was made at correlating the boundary-layer-thickness parameters; however, from comparisons with solutions for a perfect gas, it was noted that there were only minor effects of dissociation and ionization. One interesting point evident in the displacement-thickness results was that very small and even negative values were indicated under conditions which simulated subsonic flow at very high static enthalpies with cold walls. These results may be of some interest in the design of hypersonic inlets and nuclear-reactor heat exchangers.

Ames Research Center  
National Aeronautics and Space Administration  
Moffett Field, Calif., June 15, 1964

## APPENDIX A

### CONVERGENCE OF THE ITERATION PROCEDURE

The over-all convergence procedure of iterating back and forth between the momentum equation and the energy equation is illustrated in figure 13. Values of  $f_\eta$  and  $g$  at large  $\eta$  are plotted against corresponding values of  $f_{\eta\eta_w}$  and  $g_{\eta_w}$ . The dashed lines indicate the selected convergence limits. The iteration procedure consists in obtaining a solution to the momentum equation using the Crocco equation to determine the state properties and transport properties. This is indicated by I in figure 13(a). We then proceed to obtain solutions for three arbitrary values of  $g_{\eta_w}$  and plot the value of  $g$  obtained for large  $\eta$  versus the guessed value of  $g_{\eta_w}$ . This is indicated by II in figure 13(b). We then draw the line connecting these results and extrapolate toward the correct outer boundary condition to obtain a fourth value for  $g_{\eta_w}$  and solve the energy equation (point designated 4 g). We then return to the momentum equation and perform a similar operation but now replace the Crocco assumption for calculating the transport properties and state properties with the results from the previous solution to the energy equation. This process continues, iterating back and forth between the momentum equation and the energy equation, until both solutions have converged within the prescribed limits. It should be noted that the high degree of accuracy obtained by the linear extrapolation was not anticipated, and is probably a result of the good approximation of the initial solution to the momentum equation from the Crocco equation.

### EFFECTS OF STARTING VALUES ON THE CONVERGENCE PROCEDURE

There was no effect, at least to four significant figures, of starting values on the final converged solutions. This is illustrated below.

#### EFFECT OF STARTING VALUES ON CONVERGENCE

$$\begin{array}{ll}
 V_\infty = 30,000 \text{ ft/sec} & T_w = 500^\circ \text{ K} \\
 \rho_e = 1 \text{ atm} & u_e = 0
 \end{array}$$

Starting values		Converged values			
$f_{\eta\eta}(0)$	$g_{\eta}(0)$	$f_{\eta\eta}(0)$	$g_{\eta}(0)$	$f_{\eta\eta}(\infty)$	$g_{\eta}(\infty)$
0.320	0.210	(9) 0.3225	(11) 0.2135	0.4487-4	0.1108-3
.300	.215	(9) .3226	(11) .2135	.4487-4	.1108-3
.280	.220	(9) .3226	(11) .2135	.4486-4	.1107-3
.270	.225	(10) .3226	(11) .2135	.4486-4	.1108-3
.260	.230	(10) .3226	(12) .2135	.4487-4	.1108-3

The numbers in parentheses indicate the total number of iterations for the given equation. Note that there is not much effect of starting values on the number of iterations; this is again a result of the high degree of linearity exhibited by a plot of  $f_{\eta\eta}$  or  $g_{\eta}$  at large values of  $\eta$  versus  $f_{\eta w}$  or  $g_{\eta w}$  at the wall.

#### EFFECT OF THE SIZE OF THE CONVERGENCE CRITERIA ON THE SOLUTIONS

The effect of the size of the convergence criteria on the converged solutions was very small. This is illustrated by a typical example below.

Convergence criteria	$f_{\eta\eta}(0)$	$g_{\eta}(0)$	$f_{\eta\eta}(\infty)$	$g_{\eta}(\infty)$
$1 \times 10^{-3}$	0.424635	0.286245	$0.1721 \times 10^{-3}$	$0.2299 \times 10^{-3}$
$5 \times 10^{-4}$	.424592	.286245	$.5022 \times 10^{-5}$	$.1246 \times 10^{-3}$
$2 \times 10^{-4}$	.424592	.285902	$.5807 \times 10^{-6}$	$.4377 \times 10^{-4}$

Note that as the convergence criteria on  $u/u_e$  and  $H/H_e$  at the outer edge of the boundary layer is decreased from  $1 \pm 1 \times 10^{-3}$  to  $1 \pm 2 \times 10^{-4}$ , the converged values of  $f_{\eta\eta w}$  change only in the fifth significant figure and  $g_{\eta w}$  changes only in the fourth significant figure. There is some improvement in these quantities at large values of  $\eta$ ; however, they are all within the prescribed limits of  $0 \pm 1 \times 10^{-3}$ . This insensitivity to the size of the convergence criteria can again be attributed to the high degree of linearity exhibited by the plots in figure 13.

The process outlined above provides for very rapid convergence; solutions were obtained in less than one-half minute on an IBM 7090 electronic digital computer. The process has also been used successfully for stagnation-point solutions, for cases involving both moderate pressure gradients and a finite velocity at the edge of the boundary layer and cases involving moderate amounts of blowing or suction at the wall. None of these results are contained in this report.

## APPENDIX B

### HEAT-TRANSFER AND SKIN-FRICTION PARAMETERS OF COMMON INTEREST

There are other heat-transfer and skin-friction parameters in use besides those described in the text. Some of these will be described below, specialized to the case of cone flow.

The Nusselt number divided by the square root of the Reynolds number,  $R_w$ , as described in the text, is

$$\frac{Nu}{\sqrt{R_w}} = \sqrt{\frac{3}{2}} \frac{g \eta_w}{1 - g_w} \quad (B1)$$

This may be rewritten in terms of the local Reynolds number,  $Re$ , as

$$\frac{Nu}{\sqrt{Re}} = \sqrt{\frac{3}{2}} \left( \frac{\rho_e \mu_e}{\rho_w \mu_w} \right) \frac{\rho_w}{\rho_e} \frac{g \eta_w}{1 - g_w} \quad (B2)$$

where

$$Re = \frac{\rho_e u_e x}{\mu_e}$$

Conversion from the parameter described by equation (B1) to that described by equation (B2) is accomplished as follows

$$\frac{Nu}{\sqrt{Re}} = \frac{Nu}{\sqrt{R_w}} \lambda_e^{1/2} \frac{\rho_w}{\rho_e} \quad (B3)$$

The Stanton number,  $St$ , is another commonly used heat-transfer parameter and is defined as

$$St = \frac{\dot{q}}{(H_e - H_w) \rho_e u_e} \quad (B4)$$

The Stanton number usually appears multiplied by the square root of a Reynolds number as

$$St \sqrt{Re} = \sqrt{\frac{3}{2}} \frac{g \eta_w}{1 - g_w} \lambda_e^{-1/2} \sigma_w^{-1} \quad (B5)$$

which can be put in terms of the parameter used in the present report as

$$\text{St}\sqrt{R_e} = \left( \frac{\text{Nu}}{\sqrt{R_w}} \right) \lambda_e^{-1/2} \sigma_w^{-1} \quad (\text{B6})$$

The quantity appearing in parentheses in the foregoing equation is the heat-transfer parameter used in the present report; all other quantities appearing in the above equations are tabulated in table II.

The only variation in the skin-friction parameter,  $c_f\sqrt{R_e}$ , which may be of interest, is to substitute  $R_w$  for  $R_e$  as follows

$$c_f\sqrt{R_w} = \left( c_f\sqrt{R_e} \right) \lambda_e^{1/2} \frac{\rho_w}{\rho_e} \quad (\text{B7})$$

where the term in parentheses is the parameter as used in the present report.

## APPENDIX C

### EFFECTS OF SMALL AMOUNTS OF NOSE BLUNTING ON SKIN FRICTION AND HEAT TRANSFER

In the strictest sense nose blunting completely invalidates the similarity assumption used in obtaining the solutions presented in this report; however, for small amounts of blunting and sufficiently far downstream from the nose (i.e., downstream of the large pressure gradient), the assumption of similarity again will probably be good. We still have to modify the pure cone results in two ways. First, the value of the parameter  $u_e^2/H_e$  has been altered because the flow has passed through a normal shock resulting in somewhat lower edge velocities. Second, the transformed coordinate  $\zeta$  can no longer be obtained directly because the integral used in defining  $\zeta$  cannot be integrated without specification of the nose geometry which will dictate the pressure history along the body and the flight conditions. Therefore, the heat transfer and skin friction would have to be obtained by applying equations (23) and (27) of the text, being sure that the values of  $g_{\eta_w}$  and  $f_{\eta_w}$  are selected for the proper values of  $u_e^2/H_e$ .

The above discussion has disregarded the problem of the vorticity interaction between the shock layer and the boundary layer. Because of the involved nature of the vorticity interaction, it is not considered here. It could, however, influence the results to a degree, depending on the amount of blunting, the shock-layer thickness, and the boundary-layer thickness.

## REFERENCES

1. Meyerott, R. E.: Radiation Heat Transfer to Hypersonic Vehicles. LMSD 2264-R1, Lockheed Aircraft Corp., Sept. 1958.
2. Allen, H. Julian, Seiff, Alvin, and Winovich, Warren: Aerodynamic Heating of Conical Entry Vehicles at Speeds in Excess of Earth Parabolic Speed. NASA TR R-185, 1963.
3. Fay, J. A., and Riddell, F. R.: Theory of Stagnation Point Heat Transfer in Dissociated Air. Jour. of Aero/Space Sci., vol. 25, no. 2, Feb. 1958, pp. 73-85.
4. Van Tassell, William, and Pallone, Adrian: Similar Solutions of the Compressible Laminar Boundary Layer Equations for Air in Equilibrium Dissociation and Ionization With and Without Injection in the Stagnation Region. RAD TM 61-22, Avco Corp., June 28, 1961.
5. Hoshizaki, H.: Heat Transfer in Planetary Atmospheres at Super-Satellite Speeds. ARS Reprint 2173-61, Oct. 1961. Also ARS Jour., vol. 32, no. 10, Oct. 1962, pp. 1544-52.
6. Howe, John T., and Viegas, John R.: Solutions of the Ionized Radiating Shock Layer Including Reabsorption and Foreign Species Effects and Stagnation Region Heat Transfer. NASA TR R-159, 1963.
7. Kemp, Nelson H., Rose, Peter N., and Detra, Ralph W.: Laminar Heat Transfer Around Blunt Bodies in Dissociated Air. Jour. Aero/Space Sci., vol. 26, no. 7, July 1959, pp. 421-30.
8. Cohen, Nathaniel B.: Boundary-Layer Similar Solutions and Correlation Equations for Laminar Heat-Transfer Distribution in Equilibrium Air at Velocities up to 41,000 Feet Per Second. NASA TR R-118, 1961.
9. Hansen, C. Frederick: Approximations for the Thermodynamic and Transport Properties of High Temperature Air. NACA TR R-50, 1959.
10. Viegas, John R., and Howe, John T.: Thermodynamic and Transport Property Correlation Formulas for Equilibrium Air From 1,000° K to 15,000° K. NASA TN D-1429, 1962.
11. Lees, Lester: Laminar Heat Transfer Over Blunt-Nosed Bodies at Hypersonic Flight Speeds. Jet Propulsion Lab., vol. 26, no. 4., April 1956, pp. 259-269, 274.
12. Crocco, Luigi: Transmission of Heat From a Flat Plate to a Fluid Flowing at a High Speed. NACA TM 690, 1932.
13. Hildebrand, F. B.: Introduction to Numerical Analysis. McGraw-Hill Book Co., N.Y., 1956.

14. Van Driest, E. R.: Investigation of Laminar Boundary Layer in Compressible Fluids Using the Crocco Method. NACA TN 2597, 1952.
15. Eckert, Ernst R. G.: Survey on Heat Transfer at High Speeds. WADC TR 54-70, Wright Air Dev. Center, Apr. 1954.

TABLE I.- TYPICAL SOLUTIONS

(a)  $u_\infty = 15.2$  km/sec;  $p_e = 1$  atm;  $T_w = 1000^\circ$  K;  $u_e^2/2He = 0.25$

$\eta$	f	$f\eta$	$f\eta\eta$	$\eta$	g	$g\eta$	h/he
0	0	0	0.246	0	0.009	0.226	0.012
.008	.000	.002	.252	.016	.013	.243	.017
.055	.000	.015	.299	.062	.025	.289	.033
.094	.001	.027	.352	.141	.051	.359	.068
.133	.003	.042	.414	.266	.102	.464	.135
.172	.005	.060	.473	.344	.141	.534	.187
.211	.007	.079	.523	.422	.186	.626	.246
.250	.011	.100	.562	.547	.278	.868	.367
.289	.015	.123	.593	.609	.337	1.024	.444
.328	.020	.147	.620	.664	.394	.993	.518
.391	.031	.187	.656	.703	.429	.801	.560
.469	.047	.239	.696	.730	.449	.655	.580
.547	.068	.295	.738	.746	.459	.620	.583
.617	.091	.349	.781	.769	.473	.593	.590
.656	.105	.380	.806	.801	.491	.579	.607
.695	.121	.412	.825	.832	.509	.575	.622
.730	.136	.441	.833	.895	.545	.575	.678
.750	.144	.457	.834	.957	.581	.576	.705
.785	.161	.487	.833	1.066	.644	.568	.780
.793	.165	.493	.832	1.191	.713	.538	.870
.824	.181	.519	.827	1.316	.777	.482	.946
.895	.219	.577	.809	1.441	.833	.408	1.000
.973	.267	.639	.776	1.566	.879	.326	1.036
1.051	.319	.698	.730	1.691	.915	.248	1.058
1.128	.376	.752	.671	1.848	.947	.167	1.074
1.286	.501	.846	.523	2.004	.968	.108	1.052
1.629	.815	.965	.185	2.160	.981	.067	.998
1.941	1.123	.995	.034	2.348	.991	.036	.991
2.254	1.435	.999	.003	2.723	.998	.009	.998
2.566	1.747	1.000	.000	2.973	1.000	.003	1.000
3.223	2.403	1.000	.000	3.254	1.000	.001	1.000
				3.535	1.000	.000	1.000

TABLE I.- TYPICAL SOLUTIONS - Continued

(b)  $u_\infty = 15.2$  km/sec;  $p_e = 1$  atm;  $T_w = 1000^\circ$  K;  $u_e^2/2H_e = 0.5$

$\eta$	$f$	$f_\eta$	$f_{\eta\eta}$	$\eta$	$g$	$g_\eta$	$h/h_e$
0	0	0	0.260	0	0.009	0.213	0.018
.016	.000	.004	.273	.016	.013	.227	.026
.086	.001	.026	.351	.062	.024	.269	.047
.133	.003	.044	.422	.125	.043	.321	.084
.180	.005	.065	.492	.219	.076	.397	.148
.219	.008	.086	.541	.312	.117	.471	.227
.258	.012	.108	.580	.406	.165	.550	.318
.297	.017	.131	.612	.500	.221	.643	.425
.336	.022	.155	.638	.594	.286	.753	.548
.375	.029	.181	.659	.687	.362	.873	.691
.453	.045	.234	.696	.734	.404	.918	.753
.531	.065	.289	.726	.781	.448	.928	.812
.609	.090	.347	.751	.828	.491	.886	.862
.687	.120	.406	.773	.875	.530	.811	.895
.766	.154	.468	.790	.922	.567	.735	.915
.844	.193	.529	.793	.961	.594	.685	.908
.922	.236	.591	.774	.992	.615	.666	.881
1.023	.300	.667	.719	1.039	.646	.645	.847
1.102	.355	.721	.663	1.102	.686	.618	.852
1.211	.437	.788	.571	1.164	.723	.588	.825
1.367	.567	.866	.427	1.289	.792	.511	.834
1.523	.707	.922	.291	1.414	.850	.418	.850
1.680	.854	.959	.179	1.539	.897	.321	.874
1.836	1.006	.980	.099	1.664	.931	.233	.902
1.992	1.60	.991	.049	1.789	.955	.160	.928
2.148	1.315	.996	.022	1.914	.972	.105	.952
2.305	1.471	.999	.009	2.102	.986	.053	.974
2.617	1.783	1.000	.001	2.414	.996	.017	.992
2.930	2.096	1.000	.000	2.727	.999	.006	.998
3.242	2.408	1.000	.000	3.039	1.000	.002	1.000
3.617	2.783	1.000	.000	3.602	1.000	.000	1.000

TABLE I.- TYPICAL SOLUTIONS - Continued

(c)  $u_\infty = 15.2$  km/sec;  $p_e = 1$  atm;  $T_w = 1000^\circ$  K;  $u_e^2/2H_e = 0.75$

$\eta$	$f$	$f_\eta$	$f_{\eta\eta}$	$\eta$	$g$	$g_\eta$	$h/h_e$
0	0	0	0.274	0	0.009	0.214	0.037
.016	.000	.064	.287	.016	.013	.229	.052
.070	.001	.022	.349	.047	.020	.258	.079
.109	.002	.036	.406	.094	.033	.299	.128
.148	.004	.053	.468	.172	.059	.367	.228
.187	.006	.073	.526	.266	.098	.449	.392
.227	.009	.094	.574	.359	.143	.528	.545
.266	.013	.118	.613	.453	.197	.608	.746
.312	.020	.147	.648	.547	.257	.685	.963
.391	.033	.200	.692	.641	.325	.752	1.180
.469	.051	.255	.723	.734	.398	.798	1.397
.547	.731	.312	.745	.828	.473	.813	1.600
.625	.998	.371	.759	.922	.549	.794	1.783
.703	.131	.431	.763	1.016	.621	.746	1.927
.781	.167	.490	.757	1.109	.688	.678	2.032
.859	.208	.549	.740	1.172	.729	.626	2.012
.937	.253	.606	.711	1.234	.766	.572	1.962
1.016	.302	.660	.670	1.297	.800	.516	1.893
1.094	.356	.710	.620	1.359	.831	.461	1.812
1.172	.413	.756	.562	1.422	.858	.408	1.717
1.250	.474	.798	.501	1.484	.882	.357	1.618
1.328	.538	.834	.438	1.609	.921	.265	1.597
1.406	.604	.866	.377	1.766	.954	.172	1.566
1.547	.729	.912	.276	1.953	.979	.093	1.421
1.703	.875	.947	.183	2.141	.991	.045	1.274
1.859	1.025	.970	.114	2.328	.997	.019	1.165
2.016	1.177	.984	.066	2.516	.999	.007	1.091
2.172	1.332	.992	.036	2.703	1.000	.002	1.048
2.328	1.487	.996	.018	2.891	1.001	.001	1.028
2.516	1.674	.998	.007	3.078	1.001	.000	1.016
2.828	1.987	.999	.001	3.234	1.001	.000	1.010
3.203	2.361	1.000	.000				

TABLE I.- TYPICAL SOLUTIONS - Continued

(d)  $u_{\infty} = 15.2$  km/sec;  $p_e = 1$  atm;  $T_w = 1000^\circ$  K;  $u_e^2/2H_e = 0.93$

$\eta$	$f$	$f_\eta$	$f_{\eta\eta}$	$\eta$	$g$	$g_\eta$	$h/h_e$
0	0	0	0.286	0	0.009	0.217	0.131
.008	.000	.002	.293	.016	.013	.232	.186
.055	.000	.017	.344	.062	.025	.277	.353
.102	.002	.035	.412	.109	.039	.320	.541
.148	.004	.056	.490	.141	.049	.379	.658
.195	.007	.081	.560	.234	.086	.439	1.141
.242	.011	.108	.614	.328	.131	.525	1.716
.289	.017	.138	.655	.422	.184	.606	2.375
.375	.031	.197	.707	.516	.245	.679	2.983
.469	.053	.265	.742	.609	.311	.735	3.508
.562	.081	.335	.760	.703	.382	.768	3.965
.656	.116	.407	.763	.797	.454	.774	4.283
.750	.157	.478	.750	.891	.526	.756	4.477
.844	.205	.547	.720	.984	.595	.719	4.523
.937	.260	.612	.676	1.078	.661	.668	4.465
1.031	.320	.673	.620	1.172	.720	.607	4.267
1.125	.386	.728	.556	1.266	.774	.539	4.015
1.219	.457	.777	.489	1.391	.836	.444	3.921
1.312	.532	.820	.421	1.578	.906	.306	4.008
1.406	.610	.856	.356	1.766	.952	.190	3.864
1.500	.692	.887	.296	1.828	.963	.158	3.303
1.594	.776	.912	.242	2.016	.985	.084	3.020
1.687	.863	.932	.195	2.203	.996	.039	2.688
1.812	.981	.953	.142	2.391	1.001	.015	2.233
2.000	1.162	.974	.084	2.578	1.002	.003	1.710
2.187	1.346	.986	.047	2.766	1.002	-.002	1.398
2.375	1.531	.993	.025	2.953	1.002	-.003	1.214
2.562	1.718	.997	.013	3.141	1.001	-.002	1.094
2.750	1.905	.998	.006	3.328	1.001	-.002	1.067
3.125	2.279	.999	.001	3.578	1.001	-.001	1.041
3.500	2.654	1.000	.000	4.016	1.000	-.000	1.000
4.062	3.217	1.000	.000				

TABLE I.- TYPICAL SOLUTIONS - Continued

(e)  $u_{\infty} = 15.2 \text{ km/sec}$ ;  $p_e = 1 \text{ atm}$ ;  $T_w = 3000^{\circ} \text{ K}$ ;  $u_e^2/2H_e = 0.5$

$\eta$	f	$f\eta$	$f\eta\eta$	$\eta$	$g$	$g\eta$	$h/h_e$
0	0	0	0.308	0	0.035	0.239	0.070
.008	.000	.002	.315	.016	.039	.247	.078
.031	.000	.010	.340	.047	.047	.263	.094
.070	.001	.024	.380	.094	.060	.287	.119
.117	.002	.043	.423	.187	.089	.335	.176
.195	.007	.078	.479	.281	.123	.384	.234
.273	.015	.117	.518	.406	.175	.457	.336
.367	.028	.168	.553	.531	.238	.547	.448
.445	.043	.212	.578	.656	.313	.656	.581
.555	.070	.277	.607	.766	.390	.744	.703
.711	.120	.375	.643	.828	.437	.753	.733
.852	.180	.467	.666	.891	.483	.711	.748
.930	.218	.519	.666	.953	.525	.641	.781
1.008	.261	.570	.653	1.016	.563	.577	.801
1.055	.288	.601	.639	1.039	.577	.561	.793
1.109	.322	.635	.619	1.070	.594	.549	.785
1.203	.384	.691	.577	1.125	.624	.535	.771
1.359	.499	.775	.490	1.187	.657	.521	.713
1.516	.625	.844	.392	1.297	.712	.492	.712
1.672	.762	.897	.294	1.422	.771	.445	.737
1.828	.905	.936	.206	1.516	.810	.401	.744
1.984	1.054	.963	.135	1.703	.877	.303	.827
2.141	1.205	.979	.082	2.016	.947	.154	.936
2.297	1.359	.989	.046	2.328	.979	.064	.980
2.453	1.514	.994	.024	2.578	.990	.029	.992
2.641	1.701	.997	.010	2.828	.995	.013	.996
2.953	2.013	.999	.002	3.078	.998	.006	.998
3.266	2.325	.999	.000	3.328	.999	.003	.997
3.578	2.638	.999	.000	3.578	.999	.001	.997
3.891	2.950	.999	.000	3.891	1.000	.001	1.002
4.266	3.324	.999	.000	4.266	1.000	.000	1.002

TABLE I.- TYPICAL SOLUTIONS - Concluded

(f)  $u_{\infty} = 24.32$  km/sec;  $p_e = 1$  atm;  $T_w = 1000^{\circ}$  K;  $u_e^2/2H_e = 0.93$

$\eta$	f	$f\eta$	$f\eta\eta$	$\eta$	g	$g\eta$	$h/h_e$
0	0	0	0.239	0	0.004	0.181	0.051
.004	.000	.001	.245	.016	.007	.208	.099
.023	.000	.006	.283	.078	.023	.305	.328
.043	.000	.012	.334	.141	.045	.396	.641
.066	.001	.021	.406	.203	.073	.502	1.037
.102	.002	.037	.502	.266	.108	.659	1.524
.129	.003	.051	.554	.312	.143	.818	2.007
.168	.005	.074	.608	.336	.163	.869	2.255
.230	.011	.114	.676	.406	.218	.667	2.940
.309	.022	.170	.767	.465	.257	.699	3.286
.371	.034	.221	.852	.590	.353	.833	4.392
.400	.041	.246	.877	.887	.623	.906	8.093
.420	.046	.264	.889	1.184	.850	.584	11.212
.439	.052	.281	.898	1.309	.912	.375	11.975
.459	.057	.299	.906	1.363	.929	.259	12.079
.494	.068	.331	.918	1.441	.945	.174	12.040
.533	.082	.367	.926	1.520	.957	.143	11.877
.572	.097	.403	.929	1.598	.968	.120	11.666
.611	.113	.439	.927	1.676	.976	.097	11.378
.682	.147	.504	.909	1.754	.983	.076	10.664
.760	.189	.574	.866	1.832	.988	.058	9.733
.838	.236	.639	.804	1.918	.992	.042	8.743
.916	.288	.699	.728	1.996	.995	.030	7.720
.994	.345	.752	.643	2.074	.997	.021	6.727
1.072	.406	.799	.556	2.223	.999	.009	5.788
1.150	.470	.839	.471	2.379	1.000	.003	4.932
1.260	.564	.885	.362	2.535	1.000	.000	3.879
1.353	.649	.915	.279	2.691	1.000	-.001	3.162
1.510	.795	.950	.172	2.801	1.000	-.001	2.295
1.744	1.021	.978	.082	3.098	1.000	-.001	1.578
2.057	1.330	.994	.027	3.223	1.000	.000	1.159
2.807	2.078	1.000	.001				

TABLE II.- TABULATION OF FLOW CONDITIONS AND PRIMARY RESULTS

(a)  $p_e = 1 \text{ atm}$ ;  $H_w = 1.06 \text{ km}^2/\text{sec}^2$ ;  $T_w = 1000^\circ \text{ K}$ ;  $\sigma_w = 0.71$

$u_\infty$ , km/sec	$H_e$ , km <sup>2</sup> /sec <sup>2</sup>	$u_e^2/2H_e$	$g_w \times 10^2$	$h_e$ , km <sup>2</sup> /sec <sup>2</sup>	$\frac{h_w}{h_e} \times 10$	$\lambda_e$	$\frac{\rho_e}{\rho_w} \times 10$	$\sigma_e$	$g_{\eta_w}$	$f_{\eta_w}$	$Nu/\sqrt{R_w}$	$cf\sqrt{Re}$	$\frac{\delta}{x}\sqrt{Re}$	$\frac{\delta^*}{x}\sqrt{Re}$	$\frac{\theta}{x}\sqrt{Re}$
4.56	10.39	0.0	10.20	10.40	1.020	0.441	1.602	0.61	0.301	0.371	0.410	1.36	2.40	0.253	0.459
4.56	10.39	.25	10.20	7.80	1.360	.496	1.942	.61	.293	.383	.400	1.33	2.52	.365	.443
4.56	10.39	.50	10.20	5.40	1.968	.599	2.541	.66	.288	.396	.393	1.25	2.72	.565	.418
4.56	10.39	.75	10.20	2.60	4.088	.829	4.607	.73	.287	.417	.391	1.12	3.34	1.26	.374
4.56	10.39	.93	10.20	.69	15.293	.124	15.252	.71	.287	.431	.391	.95	6.61	4.67	.319
9.12	41.58	.0	2.55	41.58	.255	.283	.570	.91	.254	.295	.319	1.36	2.20	.007	.453
9.12	41.58	.25	2.55	31.18	.341	.317	.765	.93	.256	.301	.312	1.31	2.36	.225	.436
9.12	41.58	.50	2.55	20.80	.511	.359	1.044	.70	.254	.308	.319	1.26	2.71	.502	.421
9.12	41.58	.75	2.55	10.40	1.022	.441	1.602	.61	.248	.320	.322	1.18	3.01	.959	.393
9.12	41.58	.93	2.55	2.78	3.823	.811	4.352	.73	.249	.337	.311	.92	4.83	2.97	.305
12.16	73.92	.0	1.43	7.39	1.437	.188	.315	.36	.244	.262	.303	1.48	.0	-.078	.495
14.59	106.44	.0	1.00	106.44	.099	.097	.228	.27	.241	.240	.298	1.89	2.50	-.123	.626
15.20	115.50	.25	.92	86.62	.123	.152	.277	.34	.226	.246	.279	1.54	2.46	.072	.515
15.20	115.50	.50	.92	57.75	.184	.234	.396	.38	.213	.260	.263	1.32	2.44	.268	.438
15.20	115.50	.75	.92	28.88	.368	.326	.818	.87	.214	.274	.264	1.17	3.02	.967	.391
15.20	115.50	.93	.92	7.65	1.389	.498	.195	.61	.217	.286	.268	.99	4.32	2.44	.330
18.24	166.32	.50	.64	83.19	.128	.162	.286	.35	.207	.237	.254	1.44	2.62	.301	.482
18.24	166.32	.75	.64	41.59	.255	.284	.570	.91	.196	.255	.241	1.17	3.03	.985	.391
18.24	166.32	.93	.64	11.20	.948	.430	1.527	.61	.203	.269	.250	1.00	4.53	2.61	.334
21.28	226.38	.75	.47	56.60	.188	.238	.405	.38	.190	.237	.234	1.19	2.94	.855	.397
21.28	226.38	.93	.47	15.18	.700	.392	1.269	.63	.190	.252	.234	.99	5.02	3.03	.330
24.32	295.68	.93	.40	19.76	.538	.364	1.079	.69	.181	.239	.222	.97	5.17	2.89	.322

TABLE II.- TABULATION OF FLOW CONDITIONS AND PRIMARY RESULTS - Continued

(b)  $p_e = 1 \text{ atm}$ ;  $H_w = 4.10 \text{ km}^2/\text{sec}^2$ ;  $T_w = 3000^\circ \text{ K}$ ;  $\sigma_w = 0.69$ 

$u_\infty$ , km/sec	$H_e$ , km <sup>2</sup> /sec <sup>2</sup>	$u_e^2/2H_e$	$g_w \times 10^2$	$h_e$ , km <sup>2</sup> /sec <sup>2</sup>	$\frac{h_w}{h_e} \times 10$	$z_e$	$\frac{\rho_e}{\rho_w} \times 10$	$\sigma_e$	$g_{\eta w}$	$f_{\eta w}$	$Nu/\sqrt{R_w}$	$c_f \sqrt{Re}$	$\frac{\delta}{x} \sqrt{Re}$	$\frac{\delta^*}{x} \sqrt{Re}$	$\frac{\theta}{x} \sqrt{Re}$
4.56	10.40	0.0	39.40	10.39	3.947	0.640	5.080	0.61	0.229	0.412	0.463	1.26	2.76	0.571	0.421
4.56	10.40	.25	39.40	7.80	5.262	.720	6.157	.61	.215	.423	.432	1.22	2.86	.740	.407
4.56	10.40	.50	39.40	5.20	7.891	.886	8.295	.66	.202	.438	.408	1.15	3.13	1.06	.379
4.56	10.40	.75	39.40	2.60	15.784	.120	14.611	.73	.192	.457	.388	1.02	4.01	2.01	.340
4.56	10.40	.93	39.40	.69	59.043	.180	48.372	.71	.186	.473	.281	.86	8.61	6.76	.290
9.12	41.58	.0	9.70	41.58	.987	.410	1.809	.91	.270	.343	.367	1.31	2.31	.094	.441
9.12	41.58	.25	9.70	31.18	1.316	.460	2.426	.93	.271	.349	.368	1.26	2.53	.331	.425
9.12	41.58	.50	9.70	20.80	1.973	.520	3.313	.70	.268	.357	.363	1.21	2.76	.628	.408
9.12	41.58	.75	9.70	8.55	4.801	.691	5.781	.61	.258	.372	.350	1.09	3.40	1.34	.369
9.12	41.58	.93	9.70	2.78	14.761	.117	13.803	.73	.256	.386	.347	.87	5.23	3.37	.293
14.59	106.44	.0	3.85	106.44	.385	.140	.724	.27	.273	.284	.348	1.86	2.55	-.076	.618
15.20	115.50	.25	3.54	86.62	.474	.220	.879	.34	.256	.292	.325	1.52	2.51	.123	.509
15.20	115.50	.50	3.54	57.77	.710	.340	1.257	.38	.239	.308	.303	1.29	2.50	.333	.432
15.20	115.50	.75	3.54	28.88	1.421	.472	2.596	.87	.239	.325	.303	1.16	3.13	1.06	.385
15.20	115.50	.93	3.54	7.74	5.299	.722	6.187	.61	.243	.339	.308	.98	4.45	2.59	.325
18.24	166.32	.75	2.42	41.59	.986	.410	1.809	.91	.222	.301	.278	1.20	3.12	1.07	.386
18.24	166.32	.93	2.46	11.20	3.662	.623	4.844	.61	.229	.319	.288	.99	4.76	2.79	.331
21.28	226.38	.75	1.81	56.60	.725	.345	1.284	.38	.217	.283	.271	1.18	2.98	.901	.393
21.28	226.38	.93	1.81	15.18	2.703	.568	4.025	.63	.217	.300	.269	.97	5.11	3.16	.326
24.32	295.68	.93	1.39	19.76	2.076	.528	3.423	.69	.208	.286	.258	.96	5.27	3.37	.319

TABLE II.- TABULATION OF FLOW CONDITIONS AND PRIMARY RESULTS - Continued

(c)  $p_e = 1 \text{ atm}$ ;  $H_w = 8.20 \text{ km}^2/\text{sec}^2$ ;  $T_w = 4200^\circ \text{ K}$ ;  $\sigma_w = 0.61$

$u_w,$ km/sec	$H_e,$ km <sup>2</sup> /sec <sup>2</sup>	$u_e^2/2H_e$	$g_w \times 10^2$	$h_e,$ km <sup>2</sup> /sec <sup>2</sup>	$\frac{h_w}{h_e} \times 10$	$z_e$	$\frac{\rho_e}{\rho_w} \times 10$	$\sigma_e$	$g_{\eta w}$	$f_{\eta \eta w}$	$Nu/\sqrt{R_w}$	$c_F \sqrt{Re}$	$\frac{\delta}{x} \sqrt{Re}$	$\frac{\delta^*}{x} \sqrt{Re}$	$\frac{\theta}{x} \sqrt{Re}$
4.56	10.40	0.0	79.00	10.40	7.893	0.910	8.547	0.61	0.081	0.459	0.473	1.18	2.96	0.859	0.391
4.56	10.40	.25	79.00	7.80	10.524	1.023	10.360	.61	.061	.468	.354	1.13	3.16	1.09	.376
4.56	10.40	.50	79.00	5.40	15.200	1.234	13.559	.66	.042	.478	.247	1.05	3.49	1.46	.350
4.56	10.40	.75	79.00	2.60	31.568	1.709	24.583	.73	.021	.496	.124	.93	4.67	2.72	.309
4.56	10.40	.93	79.00	.69	118.086	2.553	81.387	.71	.007	.511	.042	.78	10.46	8.72	.261
9.12	41.58	.0	19.74	41.58	1.978	.584	3.044	.91	.243	.402	.371	1.31	2.37	.200	.429
9.12	41.58	.25	19.40	31.18	2.631	.654	4.081	.93	.246	.406	.374	1.23	2.57	.448	.413
9.12	41.58	.50	19.40	20.80	3.945	.740	5.573	.70	.242	.415	.368	1.18	2.88	.771	.396
9.12	41.58	.75	19.40	8.55	9.601	.982	9.726	.61	.229	.429	.348	1.06	3.60	1.57	.357
9.12	41.58	.93	19.75	2.78	29.521	1.671	23.224	.73	.223	.445	.340	.85	5.64	3.82	.282
14.59	106.44	.0	7.70	106.44	.771	.199	1.218	.27	.274	.333	.364	1.83	2.60	-.003	.608
15.20	115.50	.25	7.08	86.62	.947	.313	1.479	.34	.256	.342	.337	1.50	2.52	.191	.499
15.20	115.50	.50	7.08	57.77	1.420	.483	2.115	.38	.237	.360	.312	1.27	2.62	.420	.425
15.20	115.50	.75	7.08	28.88	2.841	.671	4.368	.87	.235	.380	.310	1.14	3.29	1.21	.379
15.20	115.50	.93	7.00	7.72	10.628	1.028	10.431	.61	.239	.394	.315	.95	4.76	2.85	.320
18.24	166.32	.75	4.93	41.59	1.973	.583	3.043	.91	.223	.356	.287	1.14	3.22	1.16	.380
18.24	166.32	.93	4.93	11.12	7.380	.888	8.189	.61	.228	.374	.294	.97	5.00	3.02	.325
21.28	226.38	.75	3.62	56.60	1.449	.490	2.161	.38	.221	.333	.281	1.17	3.01	.970	.388
21.28	226.38	.93	3.62	15.13	5.422	.808	6.783	.63	.220	.354	.279	.96	5.28	3.29	.321
24.32	295.68	.93	2.78	19.76	4.151	.750	5.760	.69	.213	.336	.268	.95	5.42	3.51	.316

TABLE II.-- TABULATION OF FLOW CONDITIONS AND PRIMARY RESULTS - Continued

(d)  $p_e = 0.1 \text{ atm}$ ;  $H_w = 4.80 \text{ km}^2/\text{sec}^2$ ;  $T_w = 3000^\circ \text{ K}$ ;  $\sigma_w = 0.65$ 

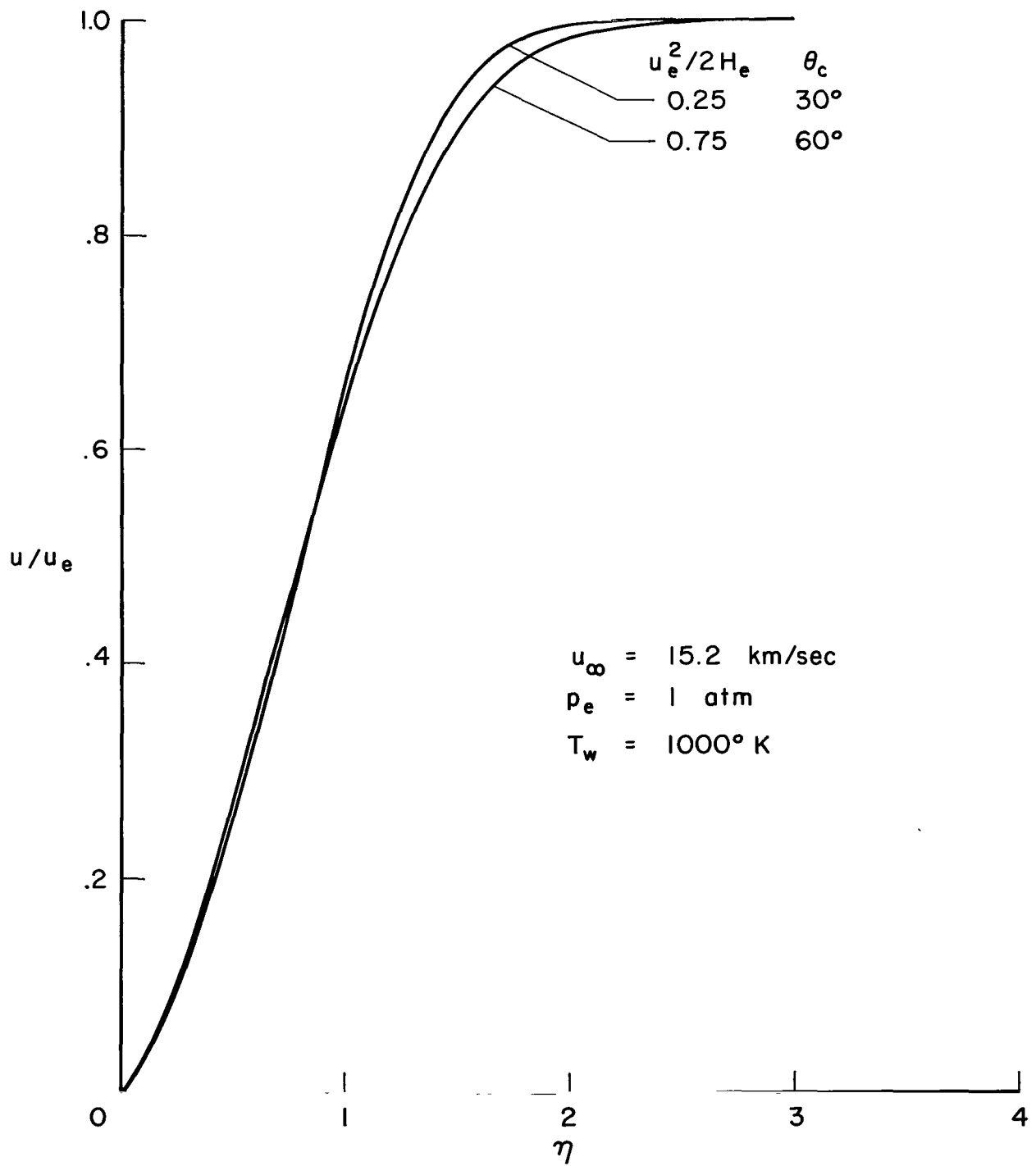
$u_{co}$ , km/sec	$H_e$ , $\text{km}^2/\text{sec}^2$	$u_e^2/2H_e$	$g_w \times 10^2$	$h_e$ , $\text{km}^2/\text{sec}^2$	$\frac{h_w}{h_e} \times 10$	$z_e$	$\frac{\rho_e}{\rho_w} \times 10$	$\sigma_e$	$g_{\eta w}$	$f_{\eta \eta w}$	$Nu/\sqrt{R_w}$	$c_f/\sqrt{Re}$	$\frac{\delta}{x} \sqrt{Re}$	$\frac{\delta^*}{x} \sqrt{Re}$	$\frac{\theta}{x} \sqrt{Re}$
4.56	10.40	0.0	46.10	10.40	4.613	0.819	5.813	0.75	0.200	0.447	0.454	1.21	2.69	0.579	0.402
4.56	10.40	.25	46.10	7.80	6.151	.891	7.122	.70	.189	.453	.429	1.18	2.85	.786	.391
4.56	10.40	.50	46.10	5.40	8.884	.975	9.215	.66	.176	.460	.400	1.14	3.13	1.10	.378
4.56	10.40	.75	46.10	2.60	18.450	1.118	14.967	.62	.157	.468	.357	1.08	4.00	1.98	.361
4.56	10.40	.93	46.10	.69	69.020	1.560	36.341	.57	.142	.475	.323	.93	7.03	5.18	.311
9.12	41.58	.0	11.55	41.58	1.153	.422	1.960	.66	.234	.373	.325	1.41	2.46	.218	.469
9.12	41.58	.25	11.55	31.18	1.537	.509	2.555	1.18	.242	.385	.335	1.32	2.53	.400	.440
9.12	41.58	.50	11.55	20.80	2.306	.629	3.535	1.00	.252	.399	.349	1.23	2.77	.664	.408
9.12	41.58	.75	11.55	8.55	5.612	.869	6.675	.71	.258	.418	.357	1.10	3.47	1.46	.365
9.12	41.58	.93	11.55	2.78	17.254	1.106	14.332	.62	.257	.430	.356	1.00	5.41	3.45	.333
15.20	115.50	.0	4.15	115.50	.415	.118	.778	.23	.259	.272	.331	1.94	2.74	.072	.644
15.20	115.50	.25	4.15	86.62	.554	.201	.971	.28	.239	.289	.306	1.58	2.52	.195	.523
15.20	115.50	.50	4.15	57.77	.830	.322	1.408	.32	.218	.309	.279	1.33	2.66	.486	.450
15.20	115.50	.75	4.15	28.88	1.660	.533	2.728	1.18	.215	.335	.275	1.12	3.24	1.21	.374
15.20	115.50	.93	4.15	7.76	6.180	.892	7.157	.70	.230	.359	.294	.93	4.99	3.07	.309
18.24	166.32	.50	2.88	83.19	.576	.213	1.003	.28	.220	.277	.277	1.47	2.64	.399	.487
18.24	166.32	.75	2.88	41.59	1.153	.422	1.960	.66	.202	.303	.255	1.14	3.19	1.14	.482
18.24	166.32	.93	2.88	11.12	4.313	.802	5.544	.76	.210	.324	.265	.89	4.92	3.09	.294
21.28	226.38	.93	2.12	15.13	3.169	.720	4.455	.85	.199	.300	.249	.87	4.90	3.09	.288
24.32	295.68	.93	1.62	19.76	2.426	.644	3.671	.38	.191	.281	.238	.86	4.97	3.10	.287

TABLE II.- TABULATION OF FLOW CONDITIONS AND PRIMARY RESULTS - Concluded

(e)  $p_e = 10 \text{ atm}$ ;  $H_w = 3.82$ ;  $T_w = 3000^\circ \text{ K}$ ;  $\sigma_w = 0.69$

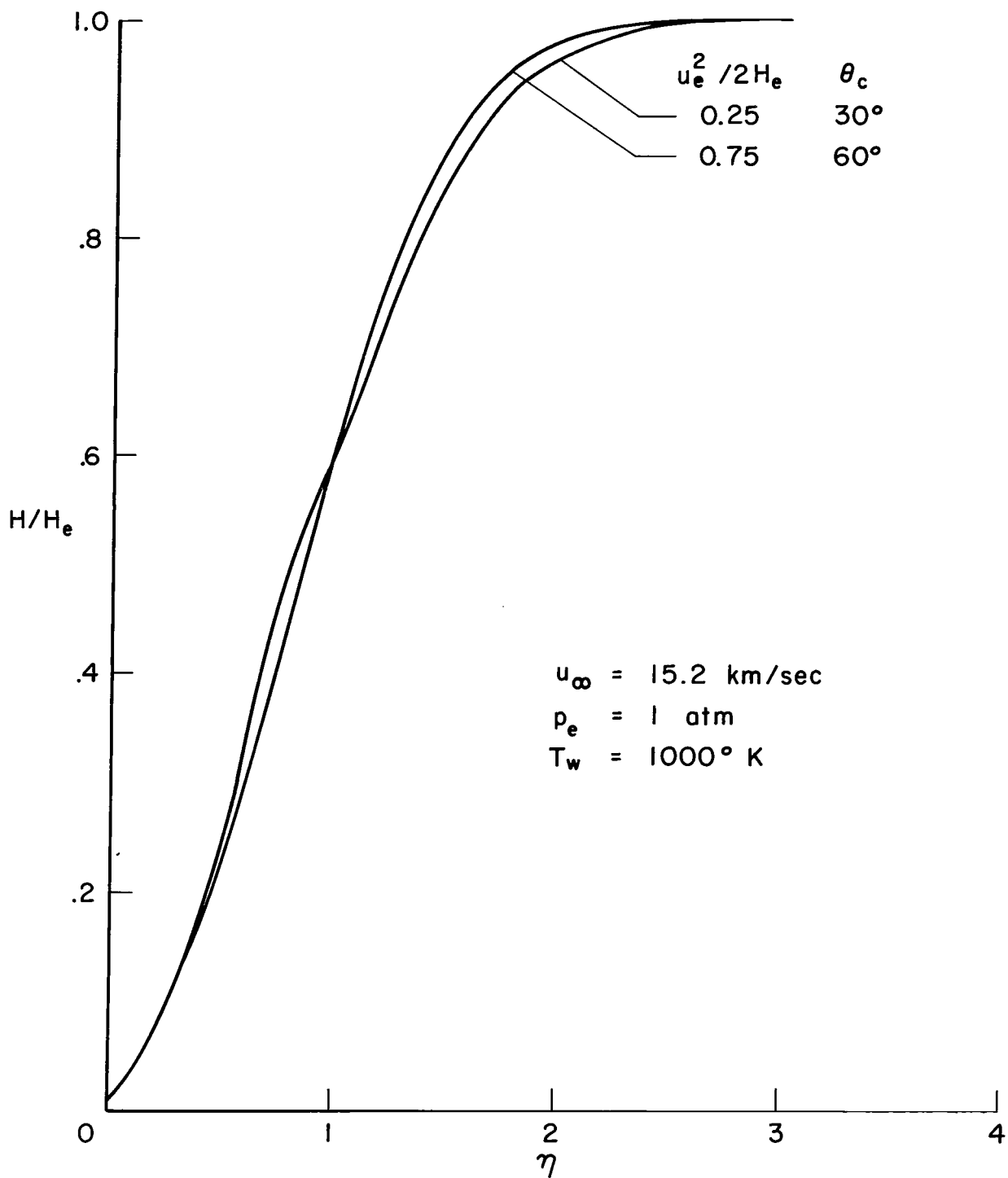
$u_{\infty}$ , km/sec	$H_e$ , km <sup>2</sup> /sec <sup>2</sup>	$u_e^2/2H_e$	$\xi_w \times 10^2$	$h_e$ , km <sup>2</sup> /sec <sup>2</sup>	$\frac{h_w}{h_e} \times 10$	$l_e$	$\frac{\rho_e}{\rho_w} \times 10$	$\sigma_e$	$\xi_{\eta w}$	$f_{\eta \eta w}$	$Nu/\sqrt{R_w}$	$cf\sqrt{Re}$	$\frac{\delta}{x} \sqrt{Re}$	$\frac{\delta^*}{x} \sqrt{Re}$	$\frac{\theta}{x} \sqrt{Re}$
4.56	10.40	0.0	36.70	10.40	3.671	0.670	4.561	0.62	0.242	0.418	0.468	1.25	2.65	0.465	0.417
4.56	10.40	.25	36.70	7.79	4.895	.744	5.708	.63	.227	.427	.439	1.21	2.79	.670	.404
4.56	10.40	.50	36.70	5.40	7.069	.861	7.612	.65	.214	.438	.414	1.16	3.04	.987	.384
4.56	10.40	.75	36.70	2.60	14.682	.118	13.535	.74	.203	.455	.393	1.03	3.91	1.89	.342
4.56	10.40	.93	36.70	.69	54.921	.201	40.772	.76	.199	.472	.385	.81	7.32	5.47	.273
9.12	41.58	.0	9.17	41.58	.918	.421	1.609	.94	.276	.351	.372	1.33	2.29	.126	.442
9.12	41.58	.25	9.17	31.18	1.224	.470	2.096	.89	.277	.358	.374	1.28	2.51	.349	.427
9.12	41.58	.50	9.17	20.80	1.835	.535	2.745	.69	.274	.367	.370	1.23	2.68	.563	.410
9.12	41.58	.75	9.17	8.55	4.466	.718	5.313	.62	.266	.383	.359	1.11	3.45	1.41	.370
9.12	41.58	.93	9.17	2.78	13.730	.115	12.840	.73	.264	.396	.356	.91	5.39	3.49	.303
12.16	73.92	.0	5.16	73.92	.869	.304	.852	.36	.276	.317	.372	1.41	2.21	-.059	.469
15.20	115.50	.50	3.30	57.77	.661	.359	1.095	.39	.313	.033	.308	1.28	2.49	.322	.427
15.20	115.50	.75	3.30	28.88	1.321	.482	2.214	.83	.244	.330	.309	1.16	3.06	1.01	.386
15.20	115.50	.93	3.30	7.74	4.929	.745	5.738	.63	.247	.344	.313	.98	4.85	2.97	.325
18.24	166.32	.75	2.29	41.59	.918	.421	1.609	.94	.227	.308	.286	1.16	3.13	1.09	.387
18.24	166.32	.93	2.29	11.12	3.432	.654	4.330	.62	.233	.324	.276	1.18	4.81	2.89	.327
21.28	226.38	.75	1.69	56.60	.674	.363	1.120	.40	.290	.222	.292	.98	2.98	.912	.393
21.28	226.38	.93	1.69	15.13	2.522	.591	3.429	.64	.221	.306	.275	.98	4.97	3.04	.324
24.32	295.68	.93	1.29	19.76	1.931	.544	2.840	.68	.213	.290	.264	.96	5.22	3.23	.323





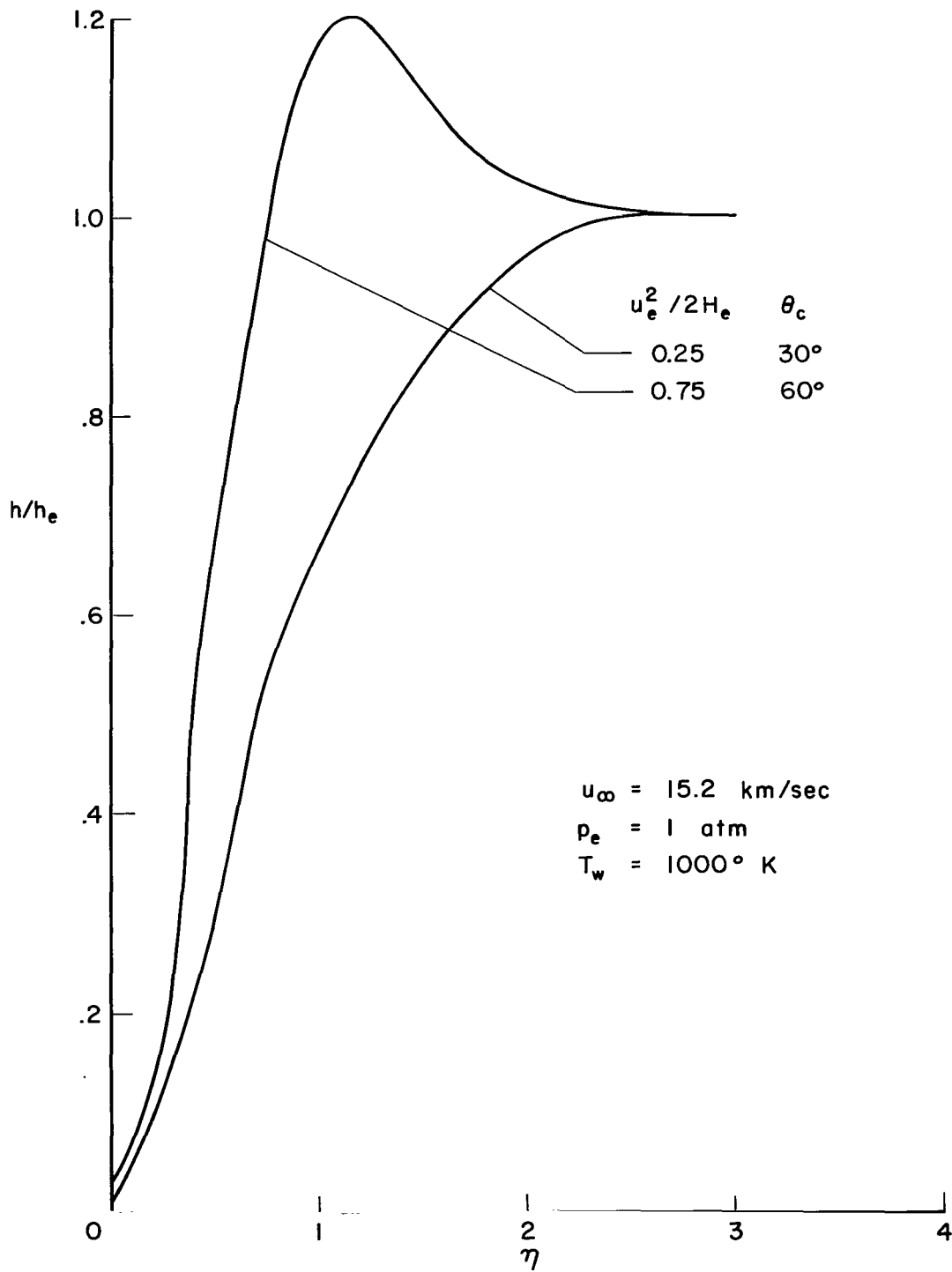
(a) Velocity profiles.

Figure 1.- Typical property profiles.



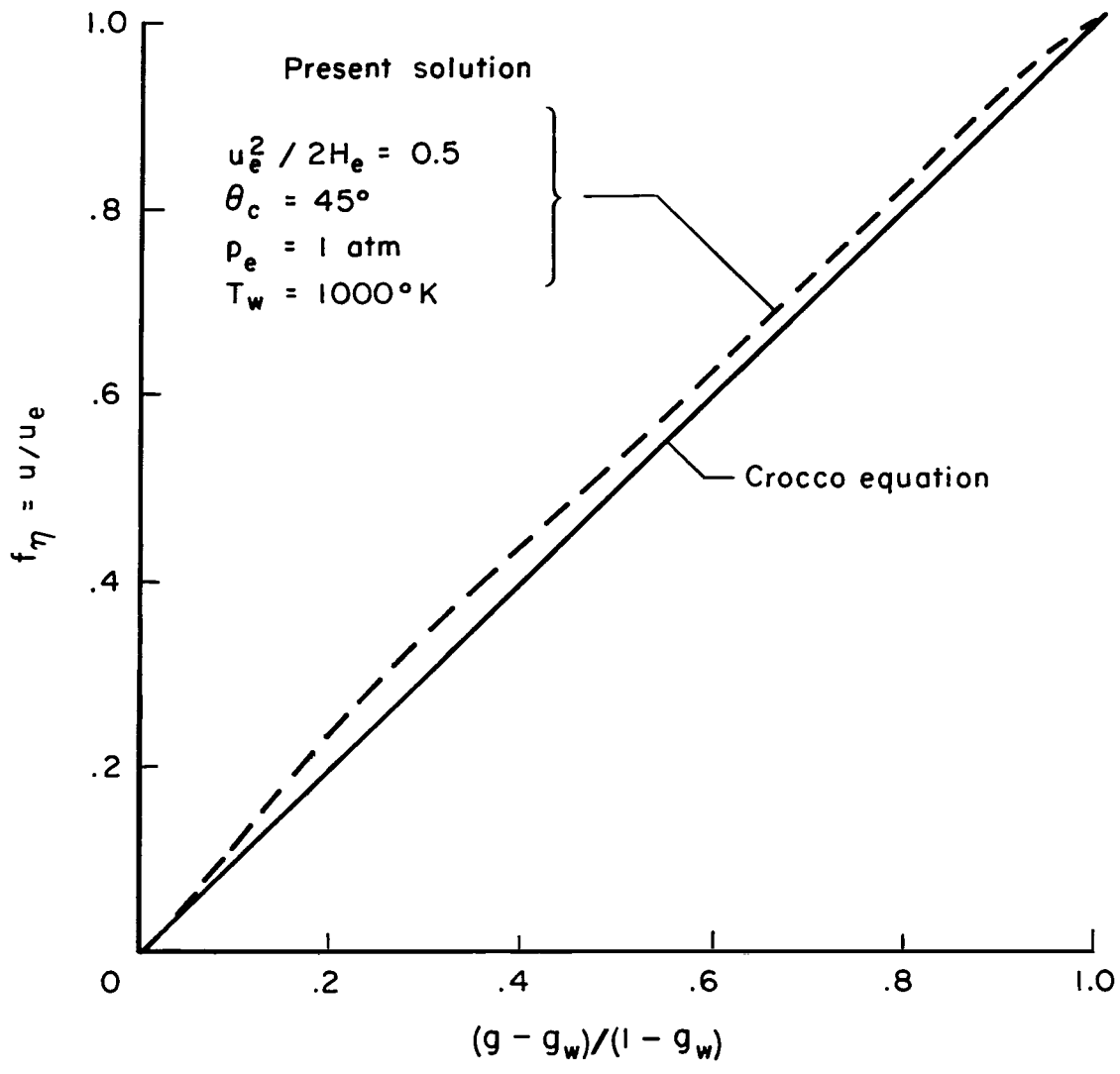
(b) Total enthalpy profiles.

Figure 1.- Continued.



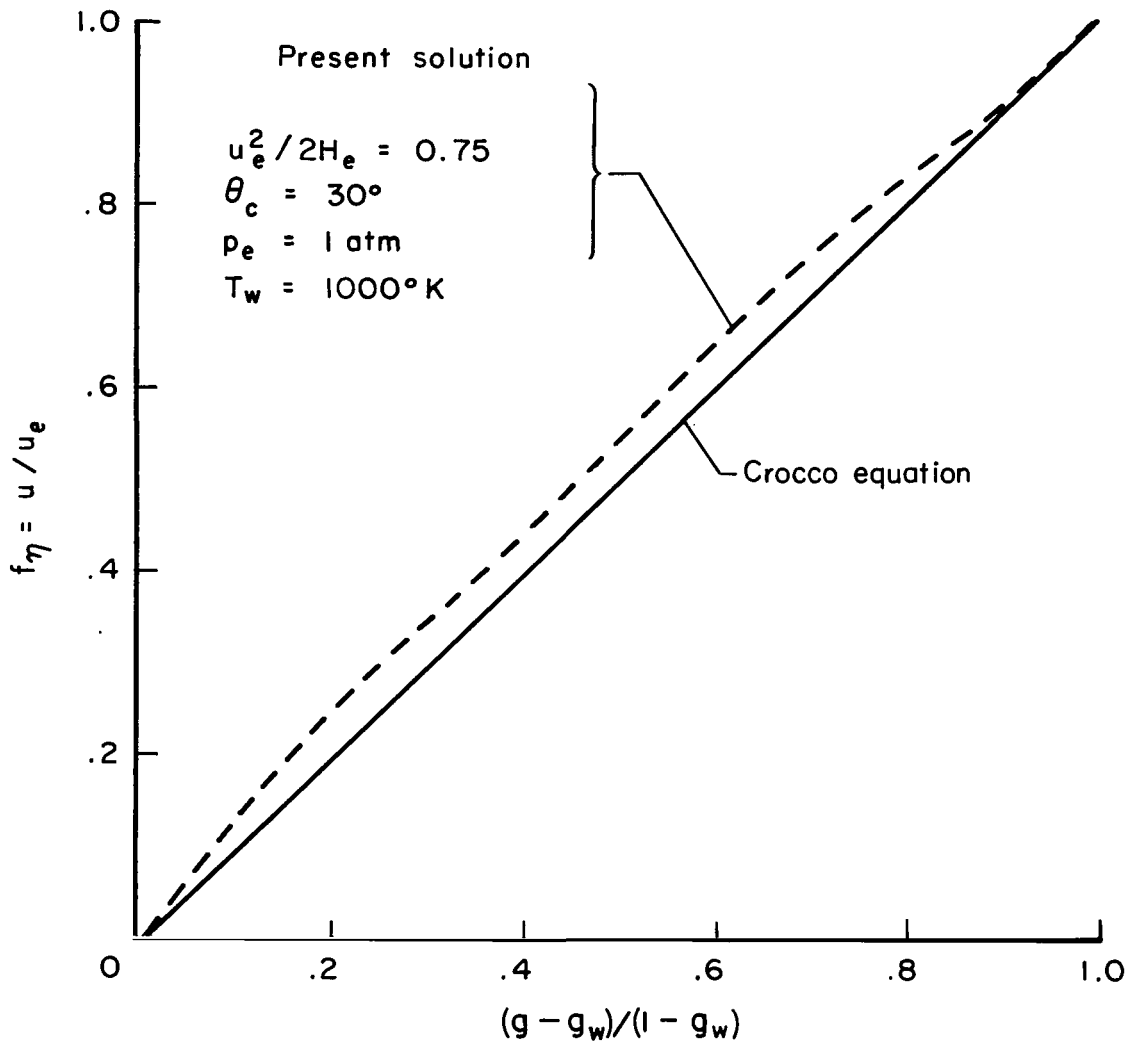
(c) Static enthalpy profiles.

Figure 1.- Concluded.



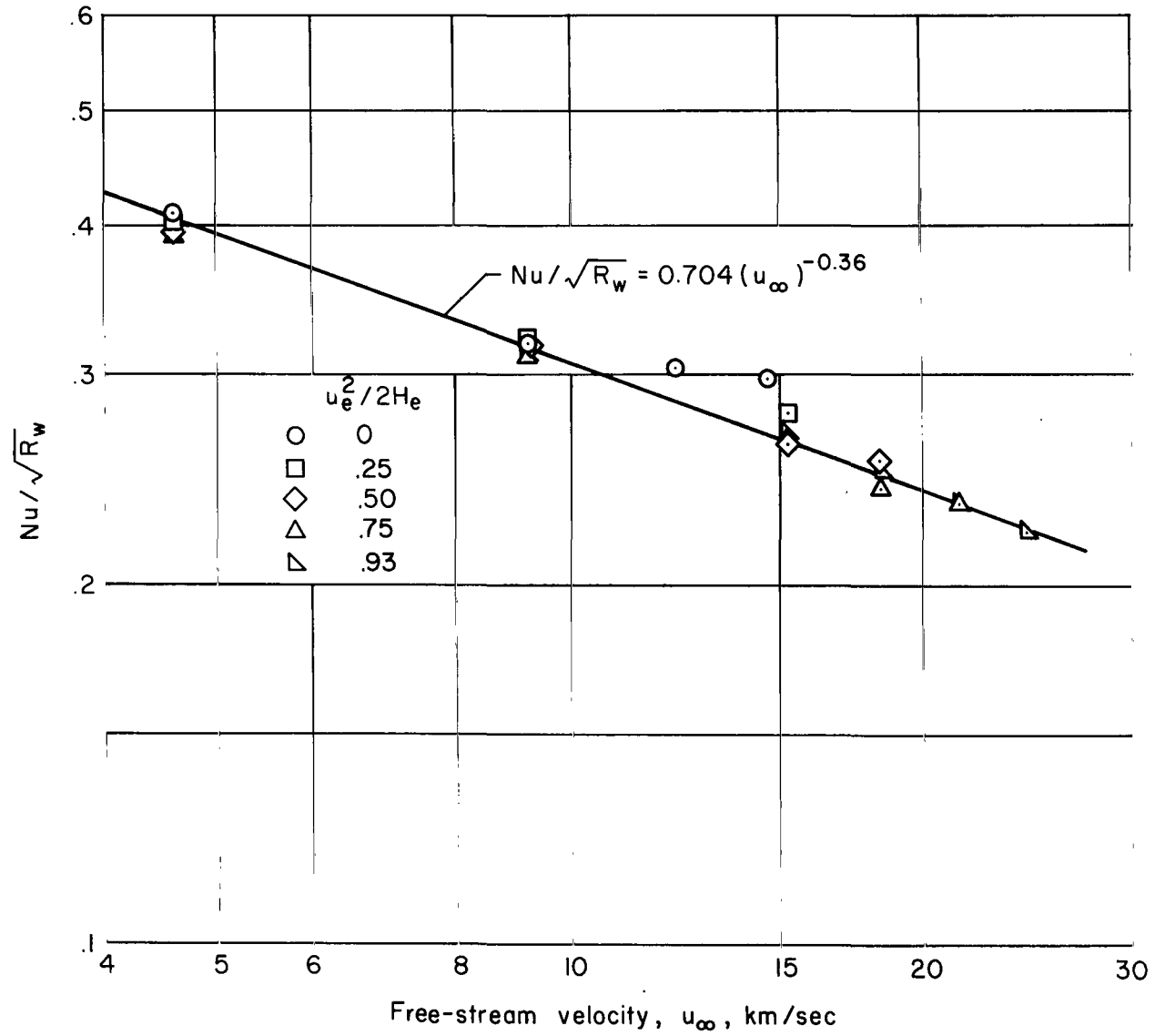
(a)  $u_\infty = 15.2 \text{ km/sec}$

Figure 2.- Comparison of exact solution with the Crocco equation.



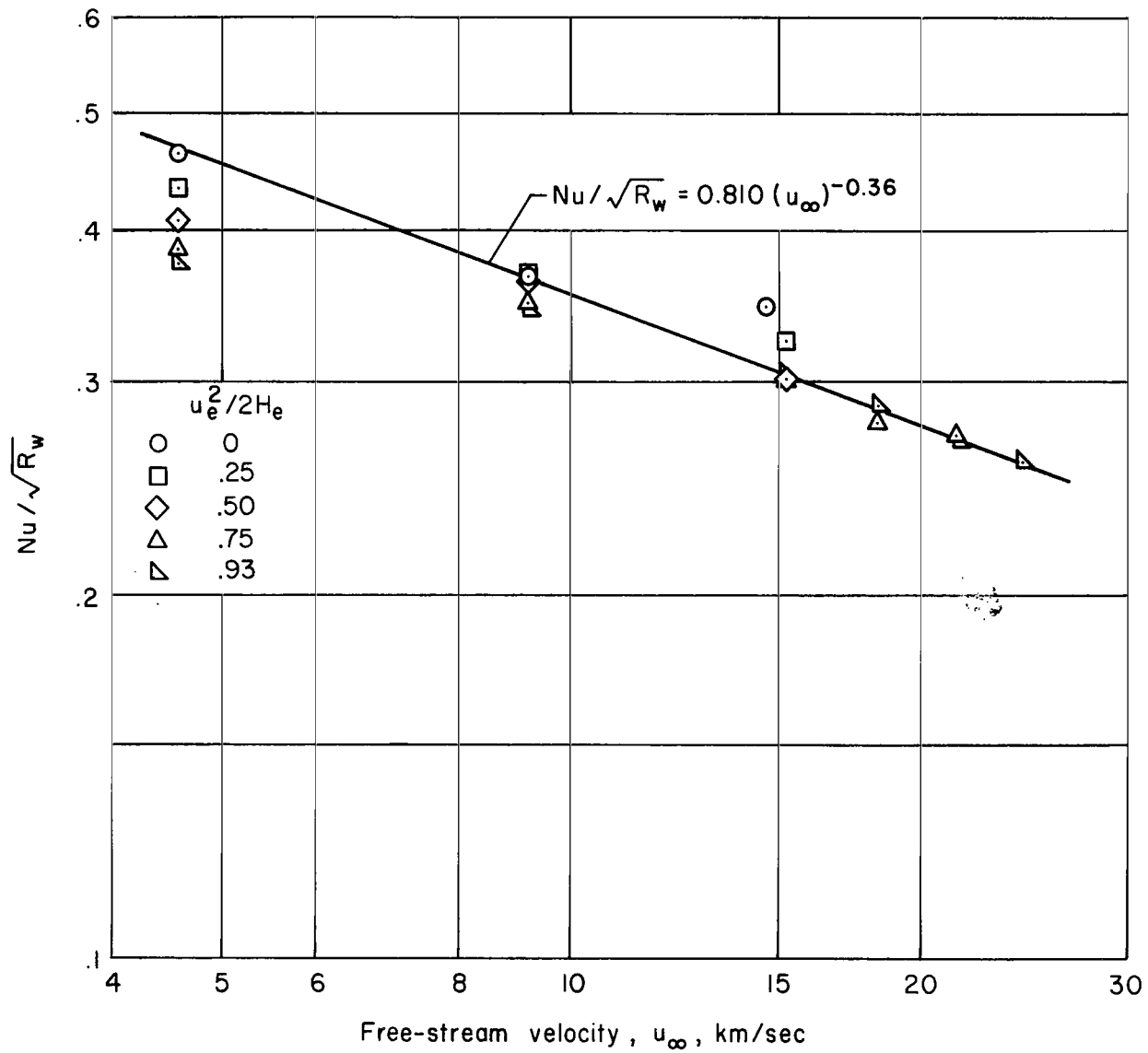
(b)  $u_\infty = 18.24 \text{ km/sec}$

Figure 2.- Concluded.



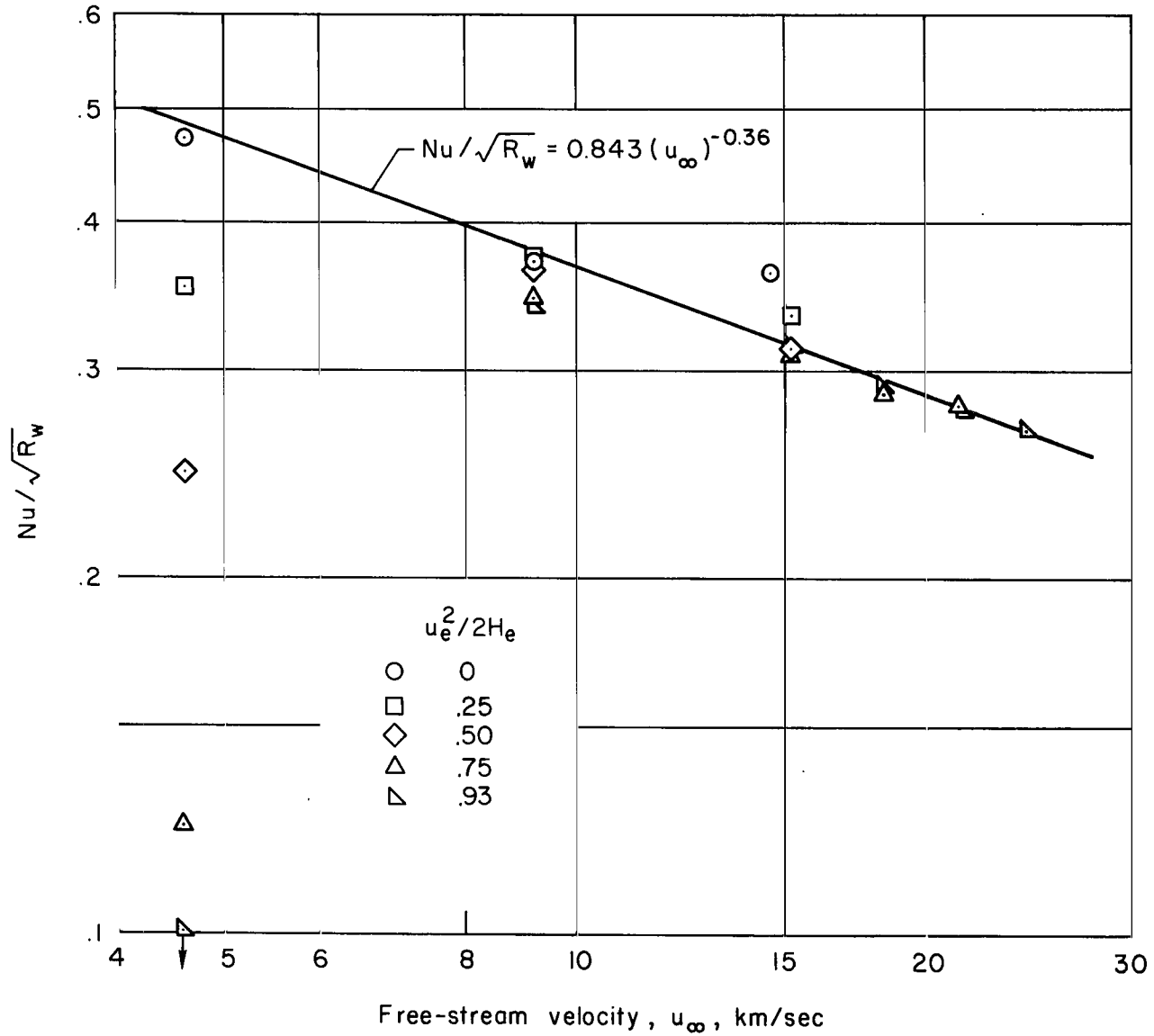
(a)  $p_e = 1$  atm,  $T_w = 1000^\circ$  K

Figure 3.- Heat-transfer results.



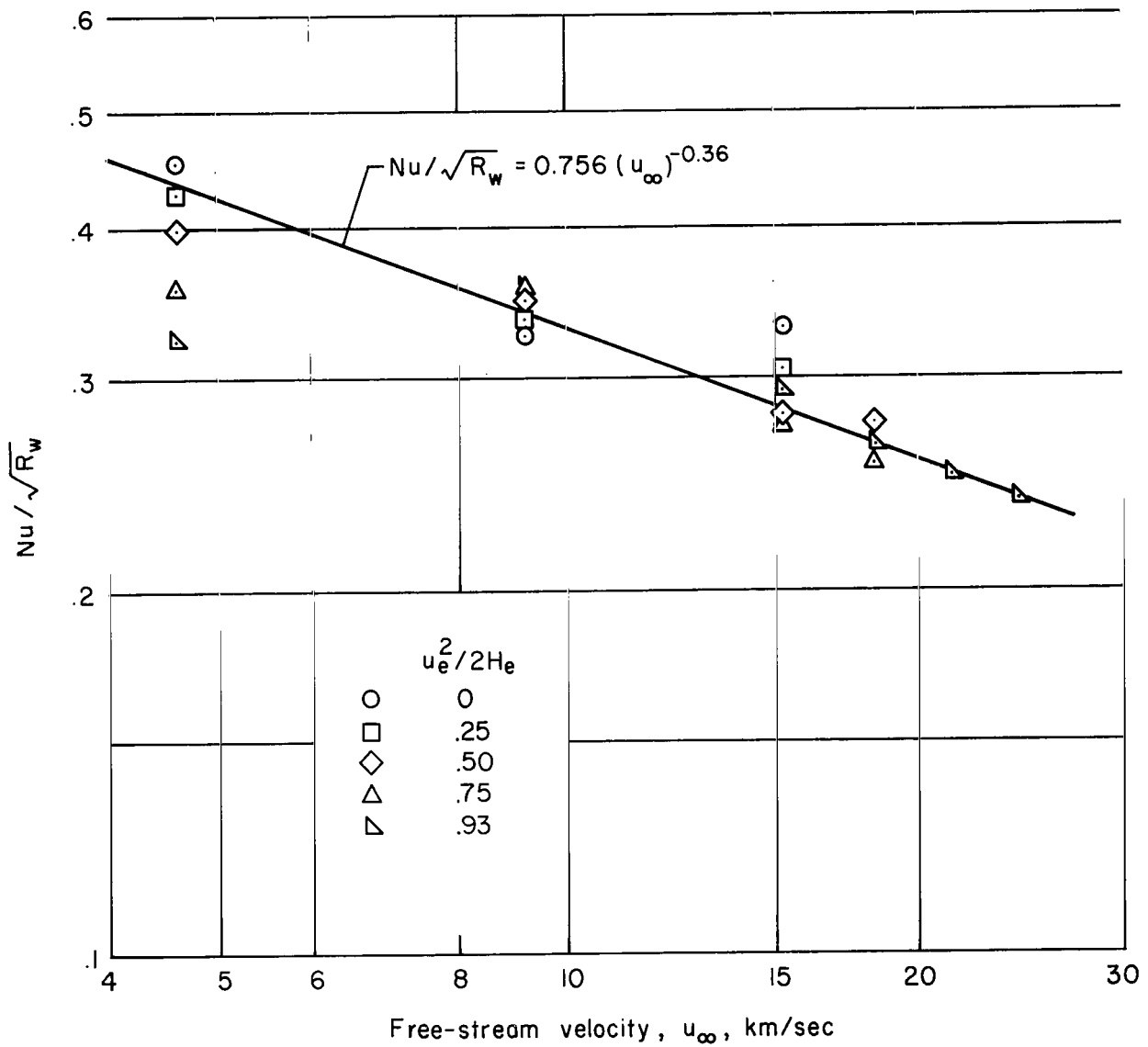
(b)  $p_e = 1 \text{ atm}$ ,  $T_w = 3000^\circ \text{ K}$

Figure 3.- Continued.



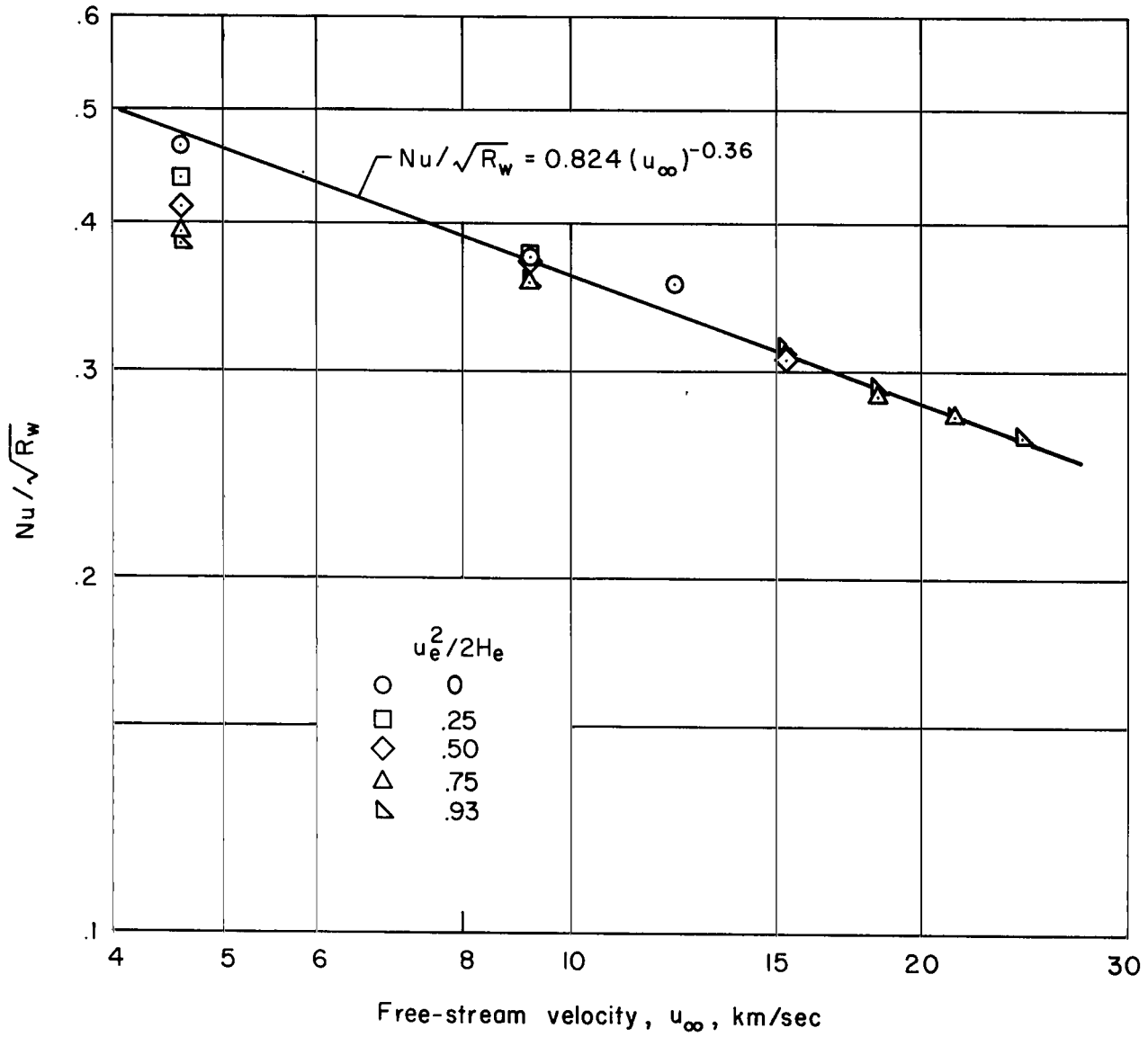
(c)  $p_e = 1 \text{ atm}$ ,  $T_w = 4200^\circ \text{ K}$

Figure 3.- Continued.



(d)  $p_e = 0.1 \text{ atm}$ ,  $T_w = 3000^\circ \text{ K}$

Figure 3.- Continued.



(e)  $p_e = 10.0$  atm,  $T_w = 3000^\circ$  K

Figure 3.- Concluded.

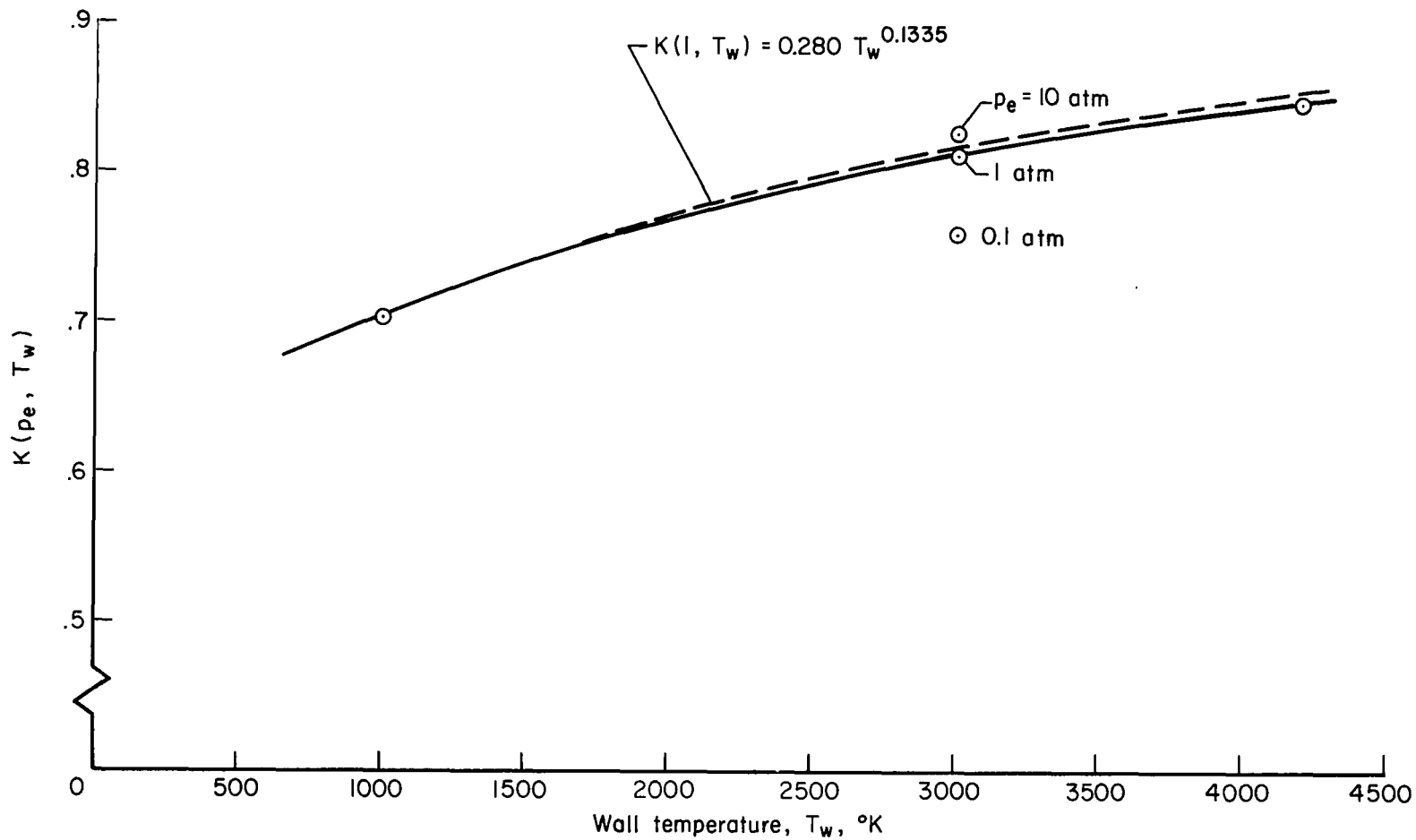
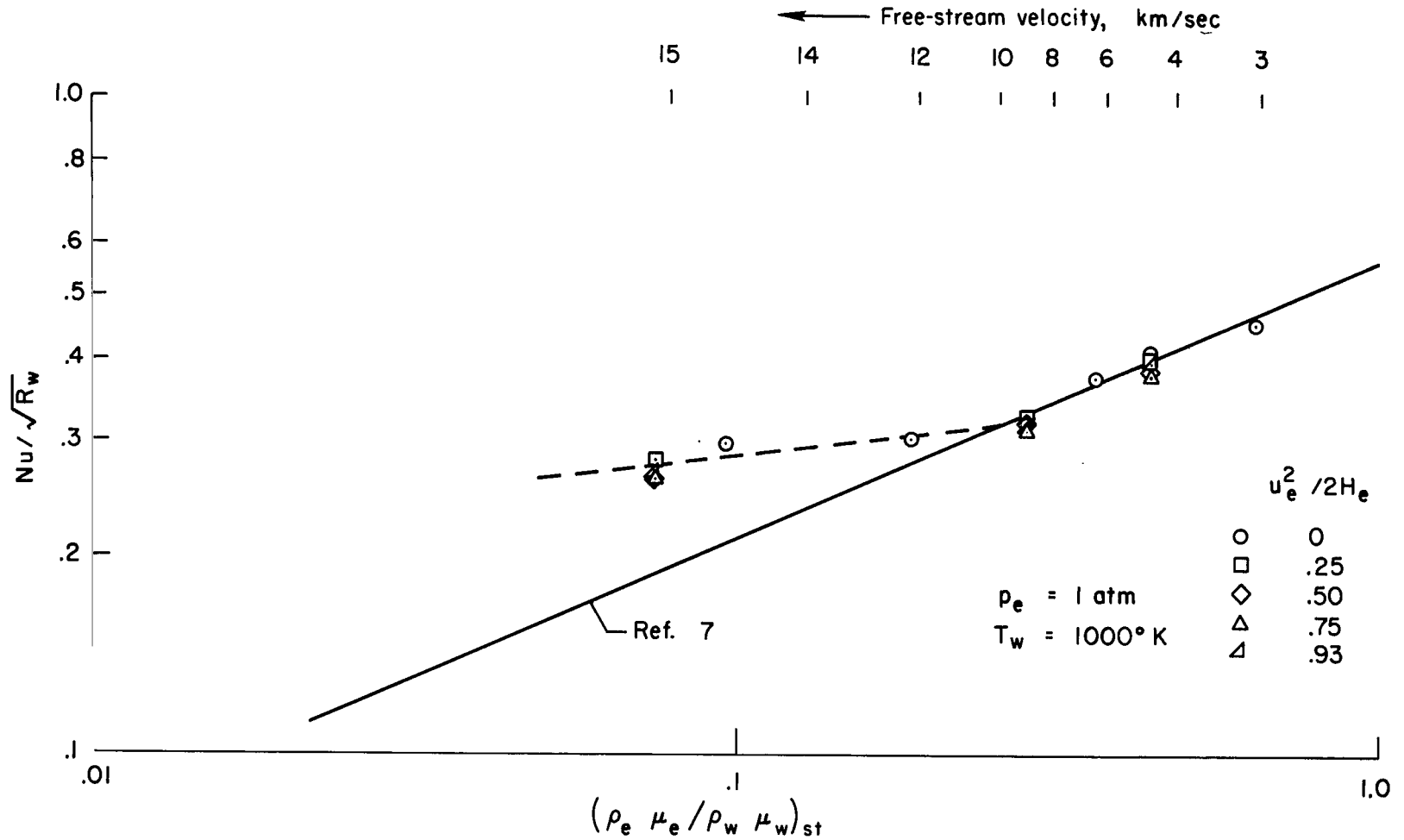
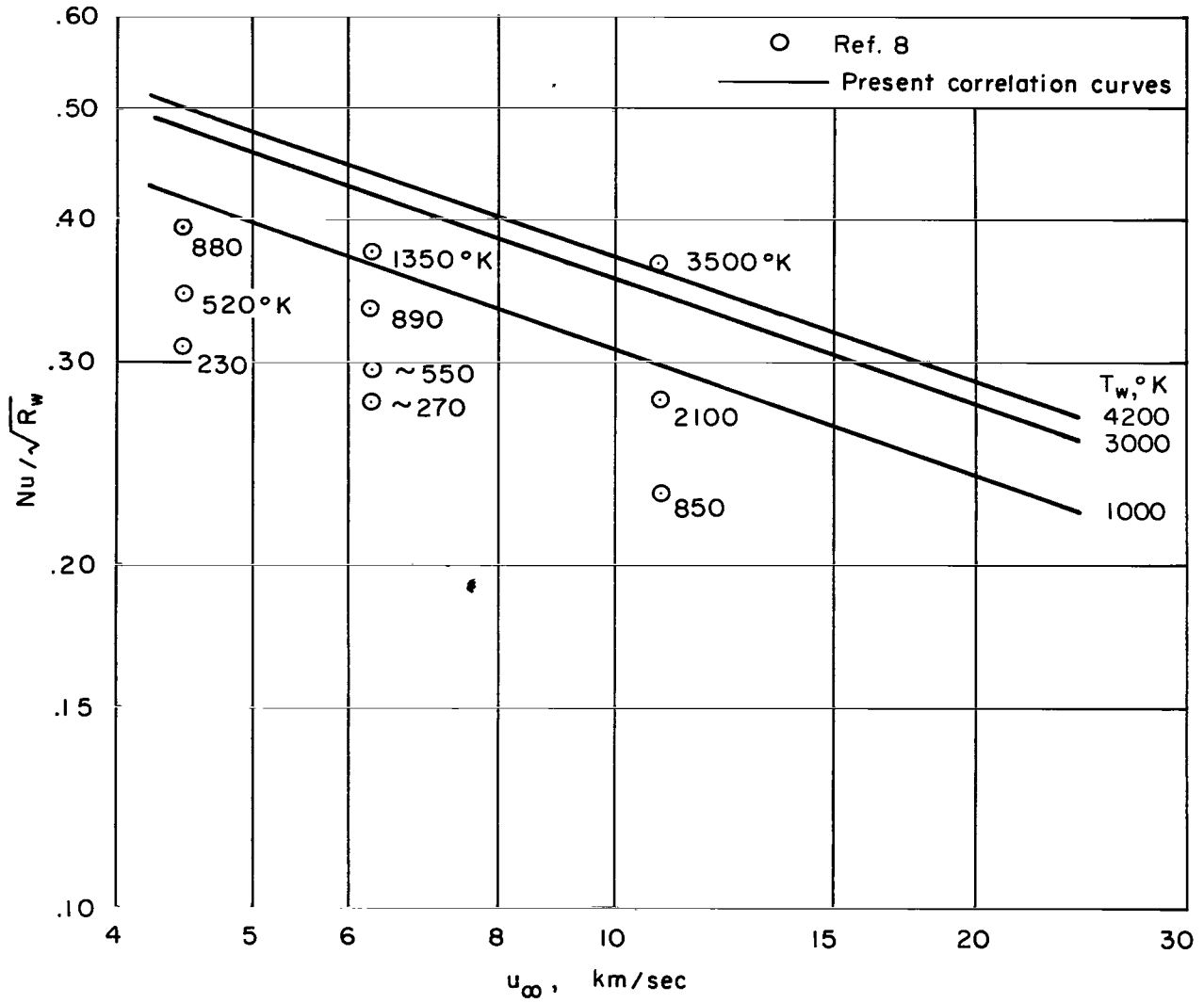


Figure 4.- The effect of wall temperature on the correlation parameter  $K(T_w, p_e)$ .



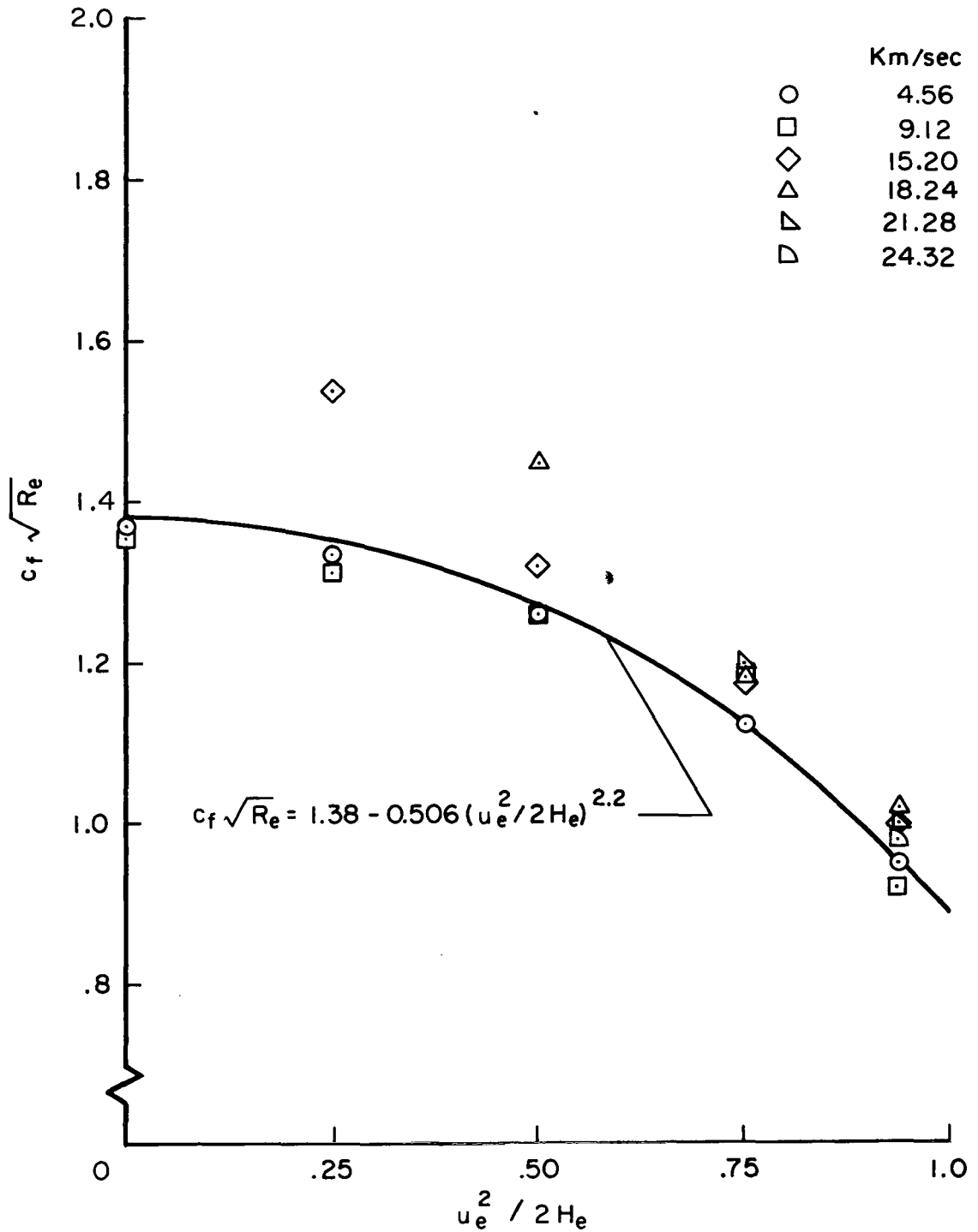
(a) Comparison with reference 7.

Figure 5.- Comparison with other theoretical heat-transfer results.



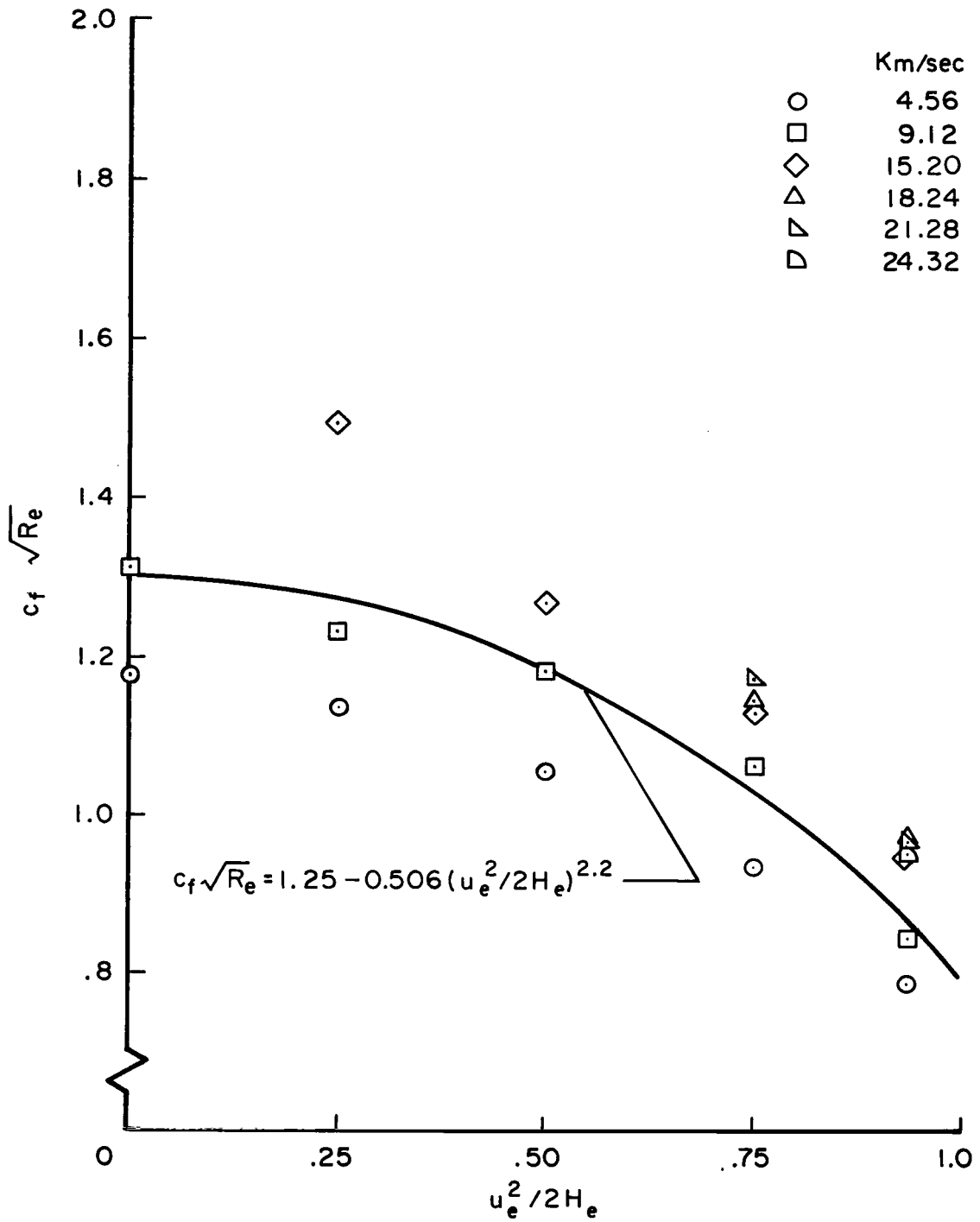
(b) Comparison with results of reference 8.

Figure 5.- Concluded.



(a)  $p_e = 1 \text{ atm}$ ,  $T_w = 1000^\circ \text{ K}$

Figure 6.- Boundary-layer skin-friction results.



(b)  $p_e = 1 \text{ atm}$ ,  $T_w = 4200^\circ \text{ K}$

Figure 6.- Concluded.

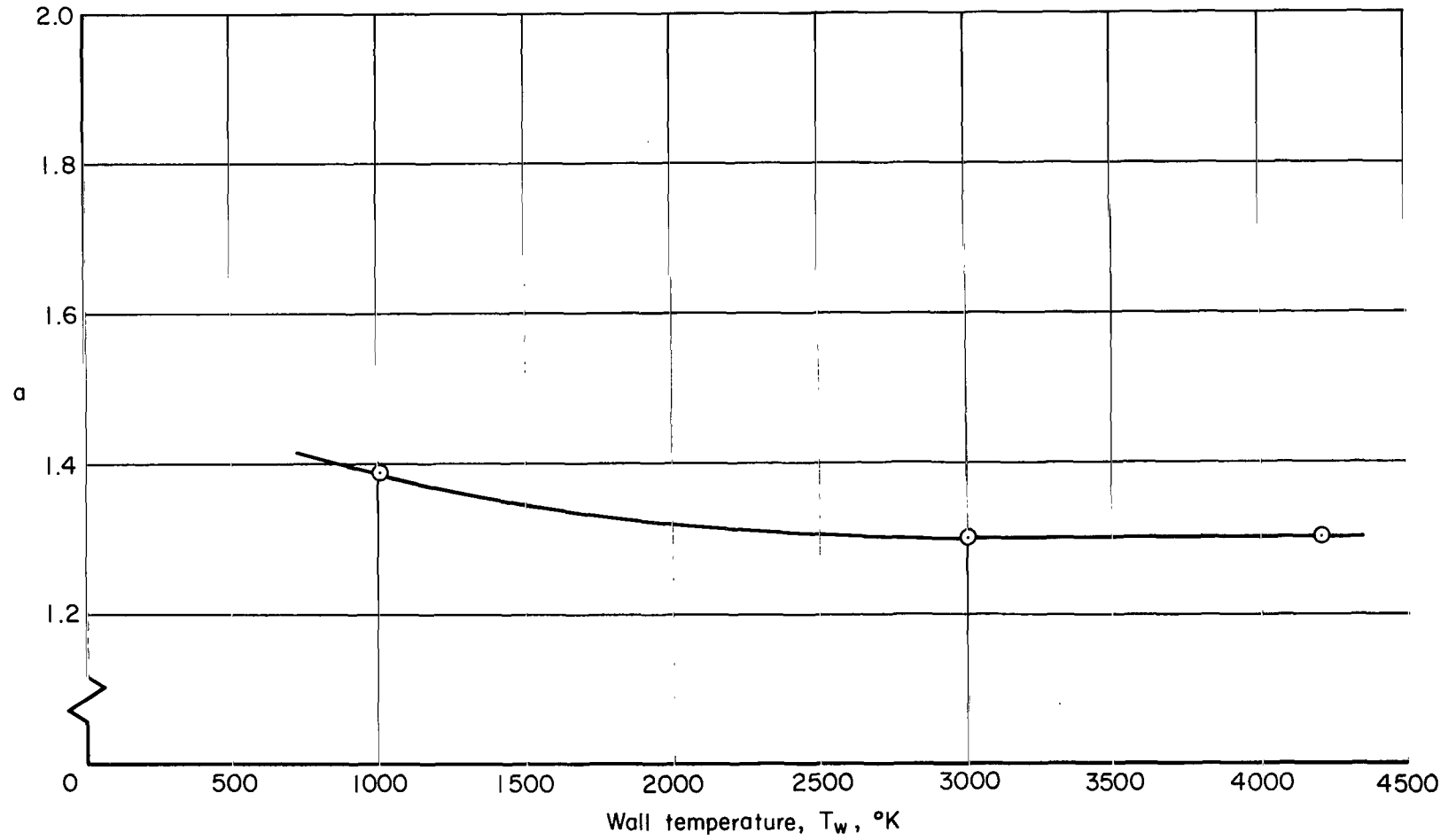
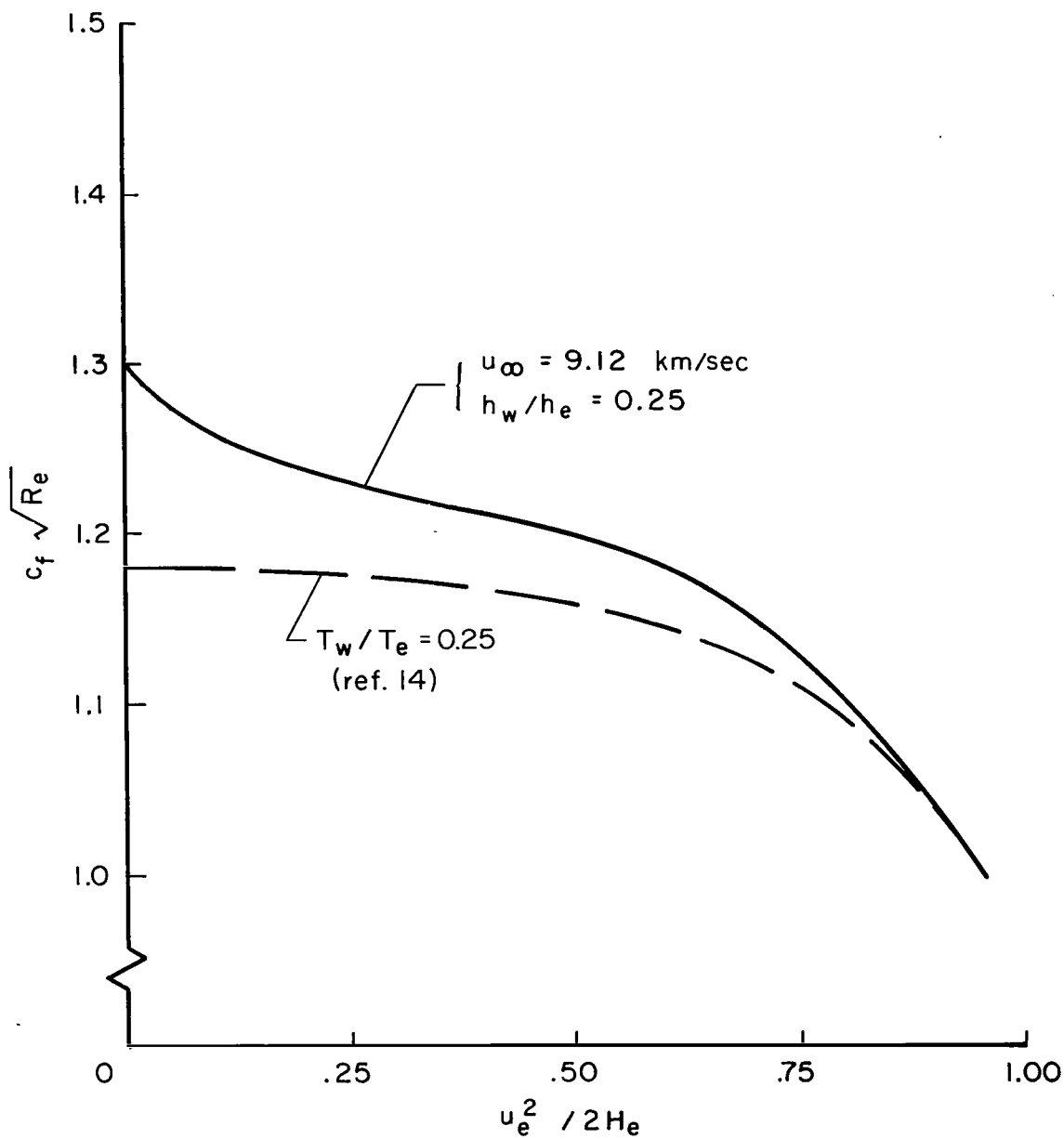
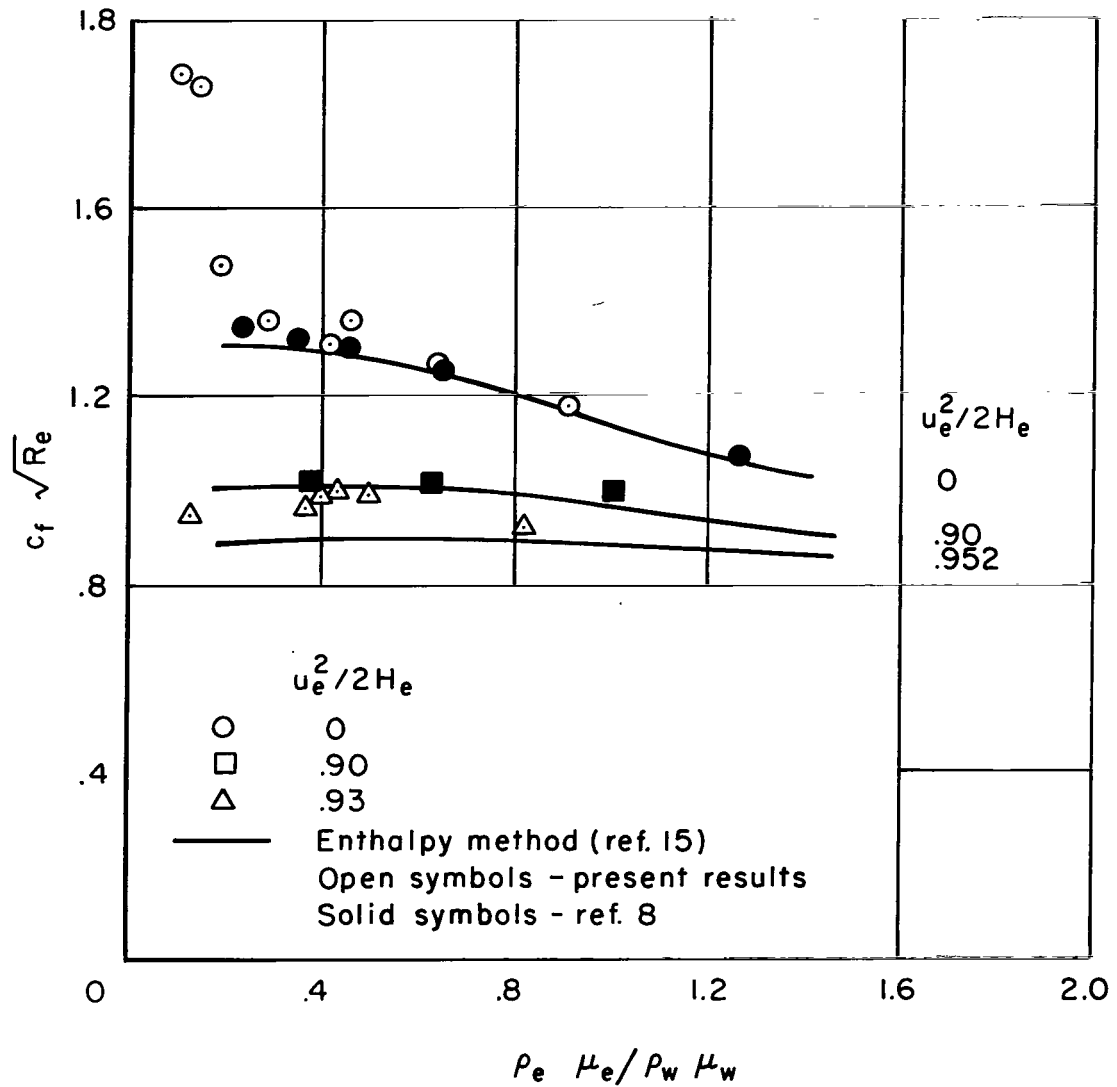


Figure 7.- The effect of wall temperature on the parameter  $a(T_w)$ .



(a) Comparison with results of reference 14.

Figure 8.- Comparison of skin-friction parameter with other theoretical results.



(b) Comparison with results of reference 8 and with the reference enthalpy method, reference 15.

Figure 8.- Concluded.

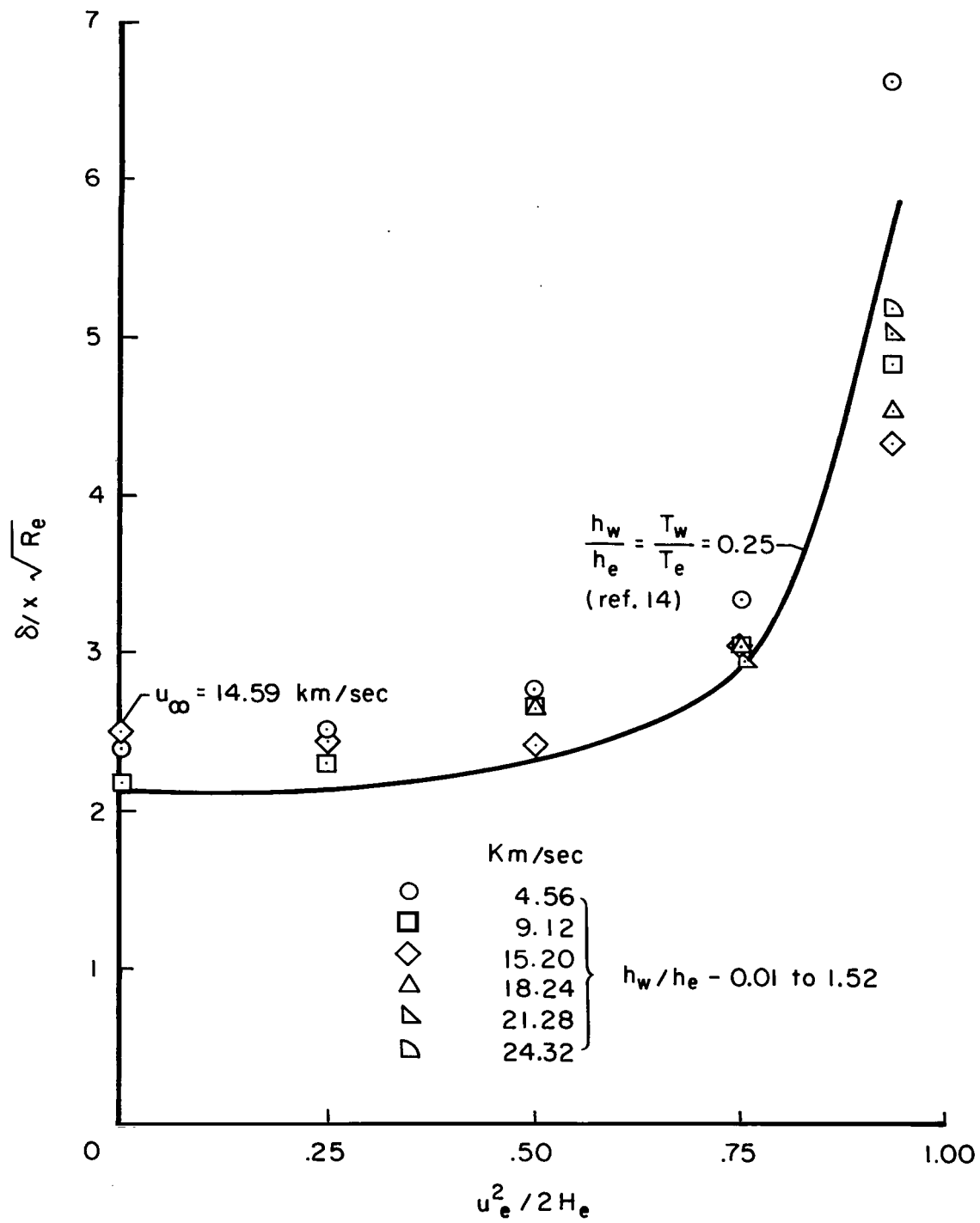


Figure 9.- Boundary-layer thickness;  $p_e = 1 \text{ atm}$ ,  $T_w = 1000^\circ \text{ K}$ .

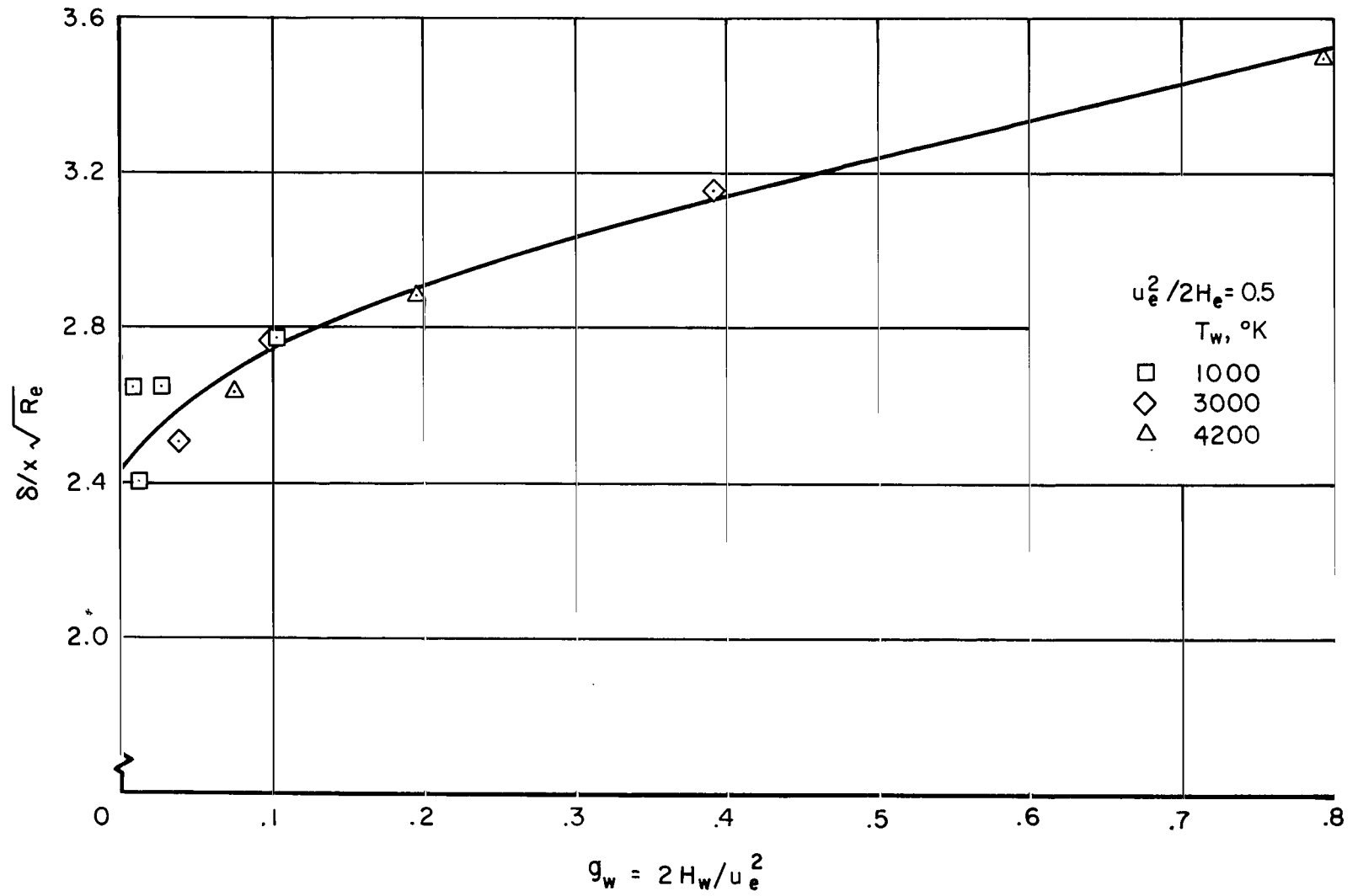


Figure 10.- The effect of the ratio wall enthalpy to total enthalpy on boundary-layer thickness.

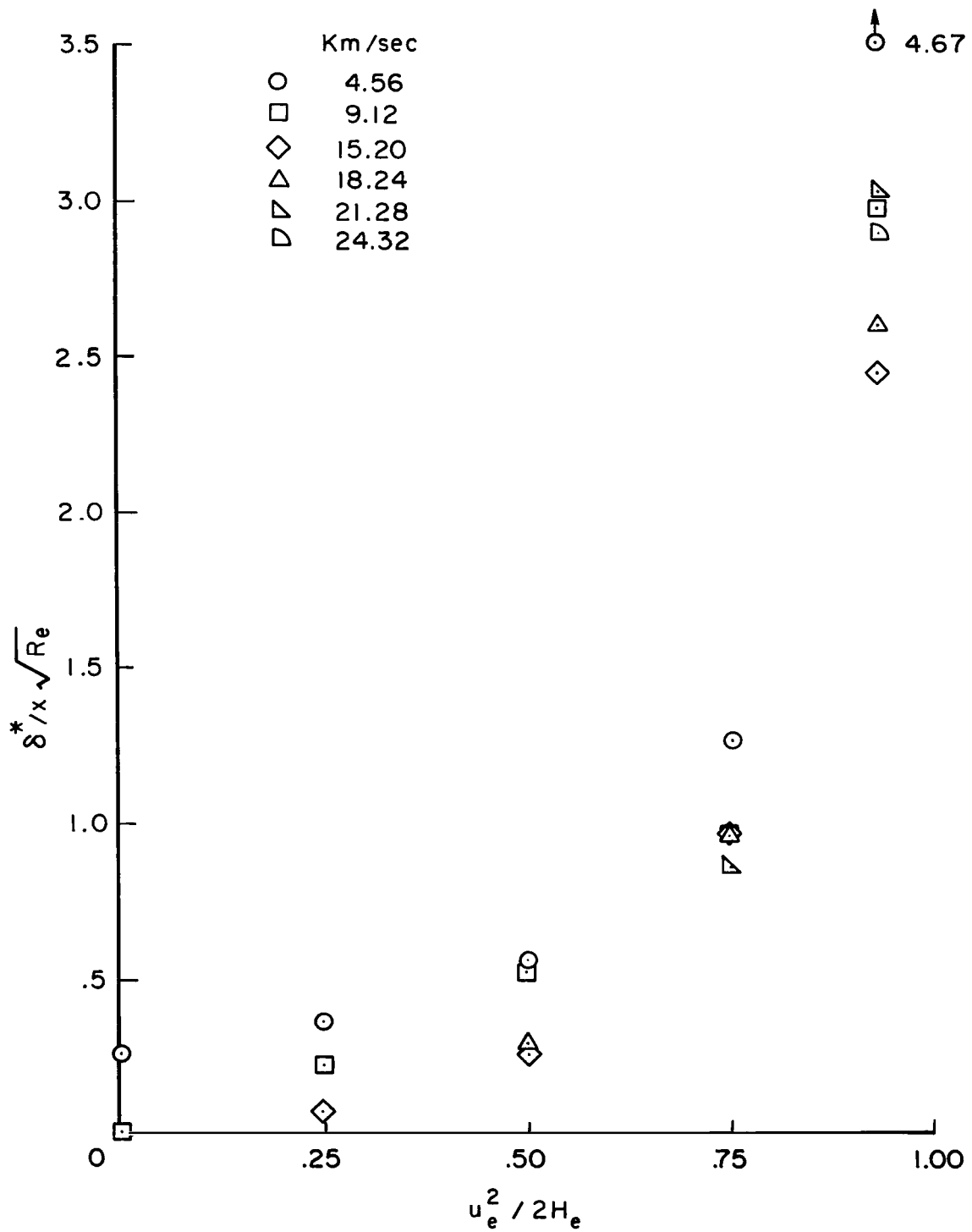


Figure 11.- Boundary-layer displacement thickness;  $p_e = 1 \text{ atm}$ ,  $T_w = 1000^\circ \text{ K}$ .

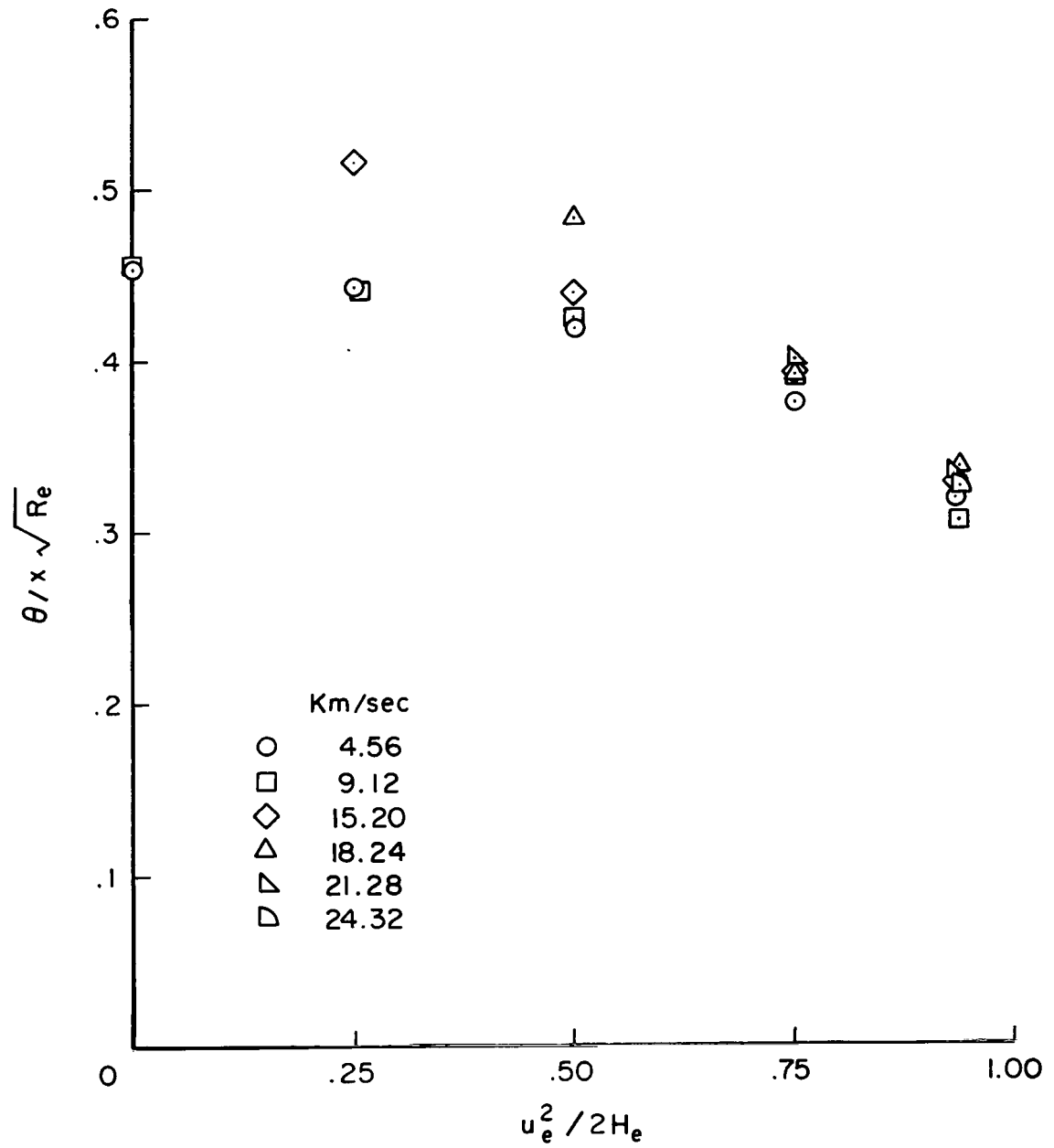
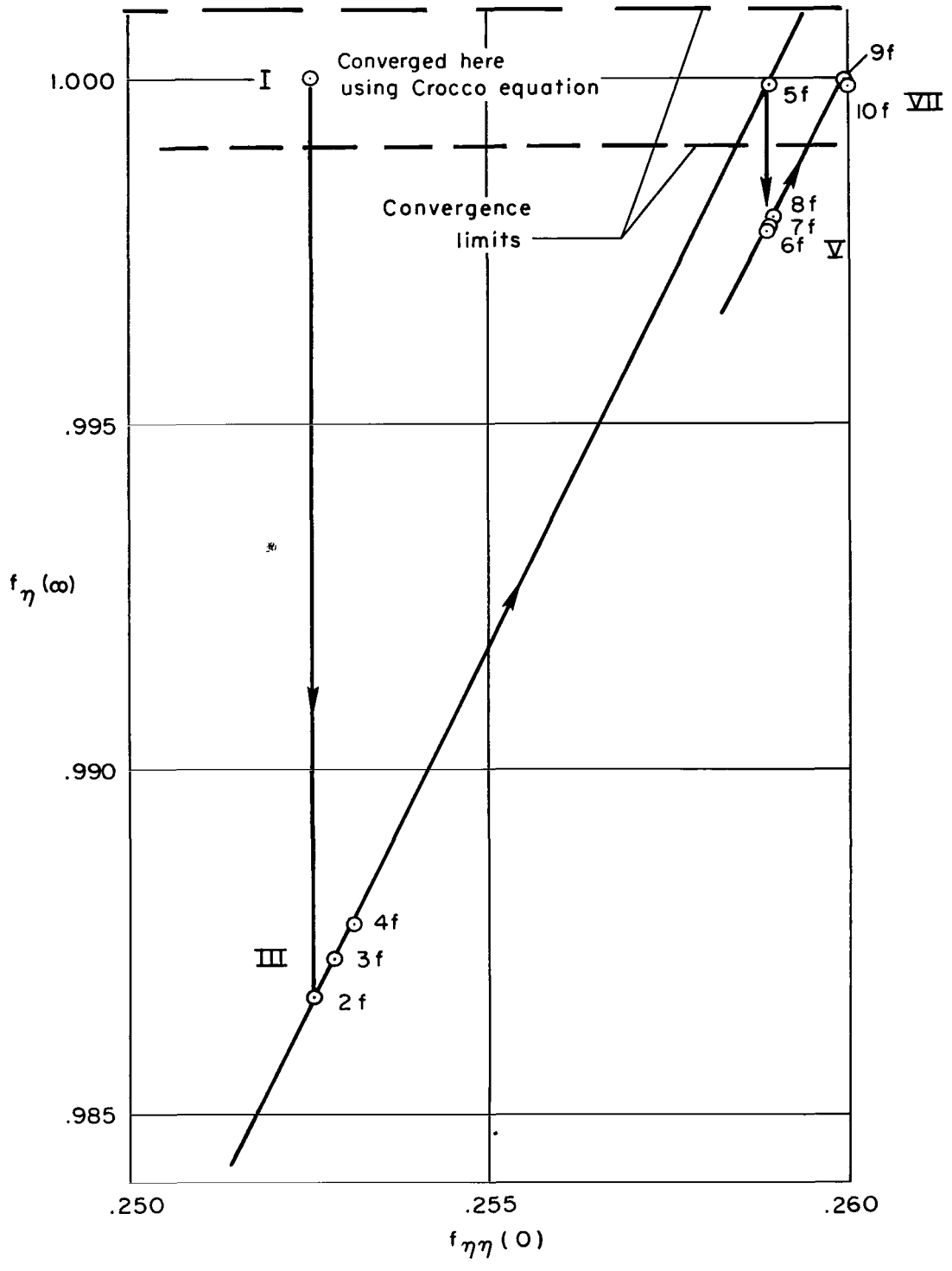
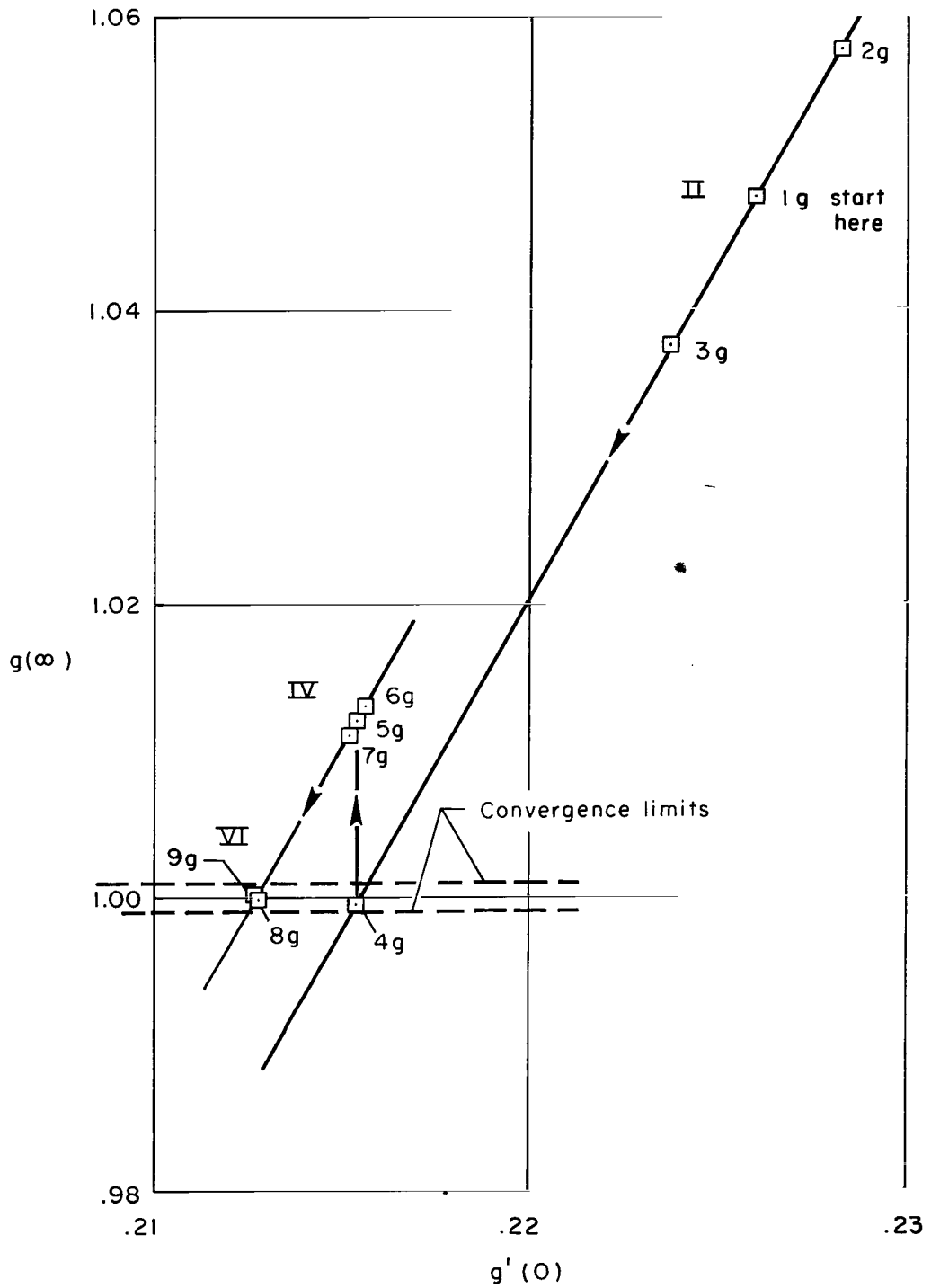


Figure 12.- Boundary-layer momentum thickness;  $p_e = 1 \text{ atm}$ ,  $T_w = 1000^\circ \text{ K}$ .



(a) Momentum equation.

Figure 13.- Typical convergence process.



(b) Energy equation.

Figure 13.- Concluded.

2.19/85  
ep

*"The aeronautical and space activities of the United States shall be conducted so as to contribute . . . to the expansion of human knowledge of phenomena in the atmosphere and space. The Administration shall provide for the widest practicable and appropriate dissemination of information concerning its activities and the results thereof."*

—NATIONAL AERONAUTICS AND SPACE ACT OF 1958

## NASA SCIENTIFIC AND TECHNICAL PUBLICATIONS

**TECHNICAL REPORTS:** Scientific and technical information considered important, complete, and a lasting contribution to existing knowledge.

**TECHNICAL NOTES:** Information less broad in scope but nevertheless of importance as a contribution to existing knowledge.

**TECHNICAL MEMORANDUMS:** Information receiving limited distribution because of preliminary data, security classification, or other reasons.

**CONTRACTOR REPORTS:** Technical information generated in connection with a NASA contract or grant and released under NASA auspices.

**TECHNICAL TRANSLATIONS:** Information published in a foreign language considered to merit NASA distribution in English.

**TECHNICAL REPRINTS:** Information derived from NASA activities and initially published in the form of journal articles.

**SPECIAL PUBLICATIONS:** Information derived from or of value to NASA activities but not necessarily reporting the results of individual NASA-programmed scientific efforts. Publications include conference proceedings, monographs, data compilations, handbooks, sourcebooks, and special bibliographies.

*Details on the availability of these publications may be obtained from:*

SCIENTIFIC AND TECHNICAL INFORMATION DIVISION  
NATIONAL AERONAUTICS AND SPACE ADMINISTRATION

Washington, D.C. 20546